

**Theoretical and experimental analyses of the temperature responses of water-saturated rocks to changes in confining pressure**

**Xiaoqiu Yang<sup>1,2</sup>, Weiren Lin<sup>3</sup>, Hehua Xu<sup>1,2</sup>, Osamu Tadai<sup>4</sup>, Xin Zeng<sup>1,2</sup>**

<sup>1</sup>Key Laboratory of Ocean and Marginal Sea Geology, South China Sea Institute of Oceanology, Innovation Academy of South China Sea Ecology and Environmental Engineering, Chinese Academy of Sciences, Guangzhou 511458, China

<sup>2</sup>Southern Marine Science and Engineering Guangdong Laboratory (Guangzhou), Guangzhou 511458, China

<sup>3</sup>Graduate School of Engineering, Kyoto University, Kyoto 615-8540, Japan

<sup>4</sup>Marine Works Japan Ltd., Nankoku 783-8502, Japan

**Corresponding author:**

Xiaoqiu Yang ([yxq2081@scsio.ac.cn](mailto:yxq2081@scsio.ac.cn)), ORCID ID: 0000-0002-3113-8796

**Key Points:**

- Theory behind the temperature responses of water-saturated rocks to stress changes under undrained and drained conditions is established
- The thermal effects of pore water predominate in water-saturated rocks (porosity>0.05), especially under undrained conditions
- The temperature response of rocks (porosity>0.05) under water-saturated and undrained conditions is greater than that under dry conditions

**Abstract**

The temperature response of water-saturated rocks to stress changes is critical for understanding thermal anomalies in the crust, because most porous rocks are saturated with groundwater. In this study, we establish a theoretical basis of the

adiabatic pressure derivative of the temperature of water-saturated rocks under both undrained ( $\beta_{\text{wet\_U}}$ ) and drained ( $\beta_{\text{wet\_D}}$ ) conditions. The value of  $\beta_{\text{wet\_U}}$  is linearly correlated with Skempton's coefficient ( $B$ ) and  $\beta_{\text{wet\_D}}$  increases nonlinearly as the pore water volume per unit volume of rock ( $\zeta$ ) increases. The theoretical calculations demonstrate that the thermal effects of pore water predominate in water-saturated rocks with medium to high porosity, especially under undrained conditions. In most cases, the temperature response of rocks with a porosity of  $\phi > 0.05$  under water-saturated and undrained conditions is greater than that under dry conditions. Experiments were also carried out on a water-saturated typical medium porosity sandstone (sample RJS,  $\phi = 0.102$ ) and on a compact limestone (sample L27,  $\phi = 0.003$ ) using an improved hydrostatic compression system. The experimental results confirm that the theoretical derivation is correct, and the calculated ranges of  $\beta_{\text{wet\_U}}$  and  $\beta_{\text{wet\_D}}$  are reliable for all 15 rocks. Consequently, this study increases our understanding of the thermal anomalies that occur after huge earthquakes, including the negative thermal anomalies, which are probably induced by co-seismic stress release, that were observed in the boreholes that penetrate seismic faults after the Chi-Chi Earthquake, the Wenchuan Earthquake, and the Tohoku Earthquake.

## **1. Introduction**

The temperature response of water-saturated rocks to stress changes is crucial for understanding the thermal anomalies that have been observed in association with various geological phenomena, such as earthquakes. *Milne* [1913] was the first to report slow temperature changes before large earthquakes. Recently, there have been increasing observations of thermal anomalies induced by seismic activity both terrestrially [*Wang and Zhu*, 1984; *Ma and Shan*, 2000; *Carreno et al.*, 2001; *Tronin et al.*, 2002; *Ouzounov and Freund*, 2004; *Wang et al.*, 2012; *Wang et al.*, 2013;

1 *Chen et al.*, 2013, 2016, 2020; *Orihara et al.*, 2014] and above/below the seafloor  
2 [*Arai et al.*, 2013; *Inazu et al.*, 2014].

3 With the exception of the positive thermal anomalies reported at fault slip interfaces  
4 in boreholes, negative thermal anomalies have been observed in the hanging wall  
5 and footwall blocks of faults after earthquakes, such as in the Chi-Chi Earthquake  
6 (1999,  $M_w$  7.6) [*Kano et al.*, 2006; *Tanaka et al.*, 2006; *Tanaka et al.*, 2007], the  
7 Wenchuan Earthquake (2008,  $M_w$  7.9) [*Li et al.*, 2013; *Li et al.*, 2015], and the  
8 Tohoku Earthquake (2011,  $M_w$  9.0) [*Fulton et al.*, 2013]. Frictional heating during  
9 earthquake faulting is known to cause positive thermal anomalies [*Tanaka et al.*,  
10 2006; *Fulton et al.*, 2013; *Li et al.*, 2015], but the causes of negative thermal  
11 anomalies have not been addressed in detail [*Yang et al.*, 2020]. In fact, changes in  
12 co-seismic stress can contribute to temperature variations. There have been several  
13 theoretical and experimental studies on the thermoelastic response of rocks and the  
14 thermodynamics of minerals [*Waldbaum*, 1971; *Richter and Simmons*, 1974; *Wong*  
15 *and Brace*, 1979; *McTigue*, 1986; *Wong et al.*, 1987; *Wong et al.*, 1988; *Stixrude*  
16 *and Lithgow-Bertelloni*, 2005; *Ma et al.*, 2007; *Mosenfelder et al.*, 2007; *Chen et al.*,  
17 2009; *Ma et al.*, 2012; *Chen et al.*, 2015]. A hydrostatic compression system has also  
18 been developed by the current authors [*Yang et al.*, 2018]. In the system, the rock  
19 specimen center can achieve adiabatic conditions during the first ~10 s after instant  
20 loading/unloading. The system was used to systematically test several representative  
21 sedimentary, igneous, and metamorphic rocks in the dry state [*Yang et al.*, 2017].  
22 These results confirm that stress release/accumulation must cause a temperature  
23 decrease/increase. In recent years, *Chen et al.* [2016, 2019] observed the co-seismic  
24 bedrock temperature responses to the Lushan Earthquake (20 April 2013,  $M_s$  7.0)  
25 and the Kangding Earthquake (22 November 2014,  $M_s$  6.3) in Sichuan, China.

26 In the field, porous rocks are usually saturated with groundwater, especially at depth.

1 Compared with dry rocks, water-saturated rocks will exhibit different temperature  
2 responses to changes in co-seismic stress. The volumetric heat capacity of water  
3 ( $(\rho c)_w$  is  $\sim 4.176 \text{ MJ}/(\text{m}^3 \cdot \text{K})$  [Lide, 2010]) is much higher than that of most dry rocks  
4 ( $(\rho c)_{\text{dry}}$  is  $\sim 1.261\text{--}2.352 \text{ MJ}/(\text{m}^3 \cdot \text{K})$ ) at room temperature [Yang *et al.*, 2017].  
5 Consequently, it is anticipated that the adiabatic pressure derivative of the  
6 temperature of rocks under water-saturated conditions ( $\beta_{\text{wet}}$ ) may be lower than that  
7 under dry conditions ( $\beta_{\text{dry}}$ ) if there is no change in pore pressure before and after an  
8 earthquake. Nevertheless, the adiabatic pressure derivative of the temperature of  
9 water ( $\beta_w$  is  $\sim 17.67 \text{ mK/MPa}$ ) is an order of magnitude greater than that of dry rocks  
10 ( $\beta_{\text{dry}}$  is  $1.5\text{--}6.2 \text{ mK/MPa}$ ) at  $\sim 20^\circ\text{C}\text{--}23^\circ\text{C}$  [Yang *et al.*, 2017]. Thus, the temperature  
11 response of pore water may be significant even if the pore pressure changes are small.  
12 In such cases, the co-seismic temperature response of water-saturated rocks under  
13 undrained conditions should be greater than that of dry rocks.

14 Since *Duhamel* [1837] and *Neumann* [1885], numerous studies on the  
15 thermoelasticity, poroelasticity, and the coupling on thermos-poroelasticity  
16 [McTigue, 1986, 1990] have been conducted, but the prior research has focused on  
17 either the temperature field influences on the stresses/strains [Carlson, 1973; Wong  
18 and Brace, 1979; Nowacki, 1986; Wang *et al.*, 1989; Hetnarski and Eslami, 2008]  
19 or the stress/strain influence on the temperature field of thermoelastic solids  
20 [Duhamel, 1837; Neumann, 1885; Biot, 1956; Lessen, 1956; Boley and Weiner, 1960]  
21 and pore pressure of porous rocks, respectively [Biot, 1941; Geertsma, 1957a].  
22 Geertsma [1957b] and Norris [1992] discussed the analogous behavior of the  
23 temperature distribution in thermoelastic problems and the pore pressure distribution  
24 in a saturated porous medium. Zimmerman [2000] presented the dimensionless  
25 parameters that quantify the coupling strength between mechanical and hydraulic (or  
26 thermal) effects. The results show that 1) for fluid-saturated rocks, the mechanical

1 deformation has a strong influence on the pore pressure; and 2) the thermoelastic  
2 coupling parameter is usually very small, so that the temperature field influences the  
3 stresses/strains, but the stresses/strains do not appreciably influence the temperature  
4 field.

5 After reviewing the theory of thermo-poroelasticity (provided in the Supporting  
6 Information), it can be found that a clear understanding of the temperature response  
7 of fluid-saturated porous rocks to changes in stress/strain has been lacking.  
8 Consequently, in this study, we analyze the theoretical basis of  $\beta$  in fluid-saturated  
9 rocks and carry out systematic experiments under undrained and drained conditions.

## 10 **2. Theoretical Analyses**

11 During most geological processes (plate motion, subduction), the pore fluid pressure  
12 ( $P_f$ ) in the crust usually changes very slowly. However, rapid changes in pore  
13 pressure can occur during some sudden geological events, such as earthquakes  
14 [Davis *et al.*, 2000; Manga *et al.*, 2003; Manga and Rowland, 2009; Davis *et al.*,  
15 2011; Manga *et al.*, 2012; Davis *et al.*, 2013; Wang and Manga, 2014; Wang and  
16 Barbour, 2017]. Therefore, this study analyzed and established the theoretical basis  
17 of the adiabatic temperature response of fluid-saturated rocks to stress changes. This  
18 was done specifically for water-saturated rocks ( $\beta_{\text{wet}}$ ) subjected to loading and  
19 unloading of a confining pressure under undrained and drained conditions. The term  
20 undrained refers to the absence of change in the pore fluid mass ( $dm_f = 0$ ) during  
21 sudden geological events; in contrast, the term drained refers to boundary conditions  
22 in which there are no pore fluid pressure changes ( $dP_f = 0$ ), such as occur during  
23 slow geological processes. For a porous rock with a porosity  $\phi$ , the factors  $(\rho c)$ ,  $(\rho c)_f$ ,  
24 and  $(\rho c)_s$  are defined as the volumetric heat capacities of the fluid-saturated porous  
25 rock, the pore fluid and the solid grains, respectively. Consequently, the volumetric  
26 heat capacity of the fluid-saturated porous rock  $(\rho c)$  can be expressed as

$$(\rho c) = (1 - \phi) \cdot (\rho c)_s + \phi \cdot (\rho c)_f. \quad (1)$$

For dry porous rocks and water-saturated porous rocks, the pores are filled with air and water, respectively. Thus, for dry porous rocks and water-saturated porous rocks,  $(\rho c)_f$  can be replaced with the volumetric heat capacity of air  $(\rho c)_a$ , and the volumetric heat capacity of water  $(\rho c)_w$ , respectively. Therefore, the volumetric heat capacity of dry and water-saturated porous rock,  $(\rho c)_{\text{dry}}$  and  $(\rho c)_{\text{wet}}$ , respectively, can be expressed as

$$\begin{cases} (\rho c)_{\text{dry}} = (1 - \phi) \cdot (\rho c)_s + \phi \cdot (\rho c)_a \\ (\rho c)_{\text{wet}} = (1 - \phi) \cdot (\rho c)_s + \phi \cdot (\rho c)_w \end{cases} \quad (2)$$

Generally, it is more convenient to measure the volumetric heat capacity of a dry rock than that of a water-saturated rock, e.g., with the transient plane source techniques [Gustafsson, 1991; ISO, 2008; Lin *et al.*, 2014; Yang *et al.*, 2017]. If the porosity  $\phi$  and volumetric heat capacity of dry rock  $(\rho c)_{\text{dry}}$  are measured, then  $(\rho c)_s$  and  $(\rho c)_{\text{wet}}$  can be calculated using the following equations:

$$\begin{cases} (\rho c)_s = [(\rho c)_{\text{dry}} - \phi \cdot (\rho c)_a] / (1 - \phi) \\ (\rho c)_{\text{wet}} = (\rho c)_{\text{dry}} + \phi \cdot [(\rho c)_w - (\rho c)_a] \end{cases} \quad (3)$$

If there is nothing within the pores, the porous rock is only a skeletal framework. Based on Equations (1) and (3), we can obtain the volumetric heat capacity of the skeletal framework of a porous rock  $(\rho c)_{\text{frm}}$

$$(\rho c)_{\text{frm}} = (1 - \phi) \cdot (\rho c)_s = (\rho c)_{\text{dry}} - \phi \cdot (\rho c)_a. \quad (4)$$

Under confining pressure  $P$ ,  $(\rho c)_{\text{frm}}$  will increase due to the reduction in the rock's volume. Thus,  $(\rho c)_{\text{frm}} = (\rho c)_{\text{frm}0} / (1 - P/K_P)$ , where  $(\rho c)_{\text{frm}0}$  is the volumetric heat capacity of the rock's skeletal framework at atmospheric pressure ( $P$  of  $\sim 0.1$  MPa),  $K_P$  is the bulk modulus of the rock under confining pressure  $P$ . In this study, the confining pressure  $P$  is less than 50 MPa. The bulk modulus of crustal rocks  $K_P$  is

up to ~5-50 GPa [Goodman, 1989; Paterson and Wong, 2005; Yang *et al.*, 2017].  
Consequently,  $(\rho c)_{\text{frm}} \approx (\rho c)_{\text{frm0}}$  since  $P/K_P$  tends to zero. Thus, in this study, the effect  
of confining pressure on the volumetric heat capacity of the rock is negligible.

## 2.1. The effective stress of fluid-saturated porous rock

In attempting to explain the time dependence of soil and sediment consolidation after  
loading, *Terzaghi* [1921] developed the notion of effective stress, which can be  
stated as  $\sigma_{zz}^{\text{eff}} = \sigma_{zz} - P_f$ . This means that the vertical effective stress  $\sigma_{zz}^{\text{eff}}$  is equal to  
the applied load  $\sigma_{zz}$  less the pore fluid pressure  $P_f$  that bears part of the load. It is  
deceptively simple [Neuzil, 2003]. *Nur and Byerlee* [1971] generalized *Terzaghi's*  
effective stress law. They assumed that the strains can be expressed as linear  
combinations of the stresses within the elastic range of deformation of a porous solid  
and are linearly related to the pore pressure. They considered an isotropic aggregate  
of solid material with connected pores of arbitrary shapes and concentration, which  
they subjected it to a confining pressure  $P_c$  and a uniform pore fluid pressure  $P_f$ .  
Subsequently, they rigorously derived the exact expressions for effective stress from  
the basic principles.

$$\begin{cases} \sigma_{ij}^{\text{eff}} = \sigma_{ij} - \alpha \cdot P_f \cdot \delta_{ij} \\ \alpha = 1 - (K/K_s) \end{cases}, \quad (5)$$

where  $\delta_{ij}$  is Kronecker's delta;  $\alpha$  is the effective stress coefficient [Gurevich, 2004],  
which is the same with the Biot-Willis coefficient for an isotropic and homogeneous  
solid (monomineral) with the pore space characterized by a smooth boundary and  
filled with a homogeneous fluid [Sahay, 2013; Müller and Sahay, 2016; Njiekak and  
Schmitt, 2019];  $K$  is the bulk modulus of the dry aggregate and  $K_s$  is the intrinsic  
bulk modulus of the solid grains. Additionally,  $K$  and  $K_s$  are demonstrated to  
represent the drained bulk modulus (i.e.,  $K = \Delta P / (\Delta V/V)|_{\Delta P_c=0}$ ) and theunjacketed

modulus (i.e.,  $K_s = \Delta P / (\Delta V/V)|_{P_c=P_f}$ ), respectively [Wang, 2000]. The volumetric strain  $\Delta V/V$  is taken to be positive in contraction, and negative in expansion.

We define compression as positive. Therefore, the effective principal stresses are

$$\begin{cases} \sigma_{11}^{\text{eff}} = \sigma_{11} - \alpha \cdot P_f \\ \sigma_{22}^{\text{eff}} = \sigma_{22} - \alpha \cdot P_f \\ \sigma_{33}^{\text{eff}} = \sigma_{33} - \alpha \cdot P_f \end{cases} \quad (6)$$

In a hydrostatic compression system, the principal stresses ( $\sigma_{11}$ ,  $\sigma_{22}$  and  $\sigma_{33}$ ) are the same to the confining pressure  $P_c$ . Thus, the effective pressure is

$$P^{\text{eff}} = (\sigma_{11}^{\text{eff}} + \sigma_{22}^{\text{eff}} + \sigma_{33}^{\text{eff}})/3 = P_c - \alpha \cdot P_f. \quad (7)$$

Equations (5)–(7) accurately describe the behavior of fluid-saturated porous rocks, and has been demonstrated by *Nur and Byerlee* [1971] under laboratory conditions. *Nur and Byerlee's* effective stress law is recognized and appears in pertinent textbooks and surveys on poroelasticity [Bourbié *et al.*, 1987; Detournay and Cheng, 1993; Wang, 2000; Neuzil, 2003; Guéguen and Boutéca, 2004; Jaeger *et al.*, 2007; Cheng, 2016; Müller and Sahay, 2019; Meng *et al.*, 2020].

If the changes in the effective pressure, confining pressure and pore pressure are defined as  $\Delta P^{\text{eff}}$ ,  $\Delta P_c$ , and  $\Delta P_f$ , respectively, then the change in the effective pressure can be expressed as

$$\Delta P^{\text{eff}} = \Delta P_c - \alpha \cdot \Delta P_f. \quad (8)$$

This provides the relationship between the changes in the effective pressure ( $\Delta P^{\text{eff}}$ ), confining pressure ( $\Delta P_c$ ), and pore pressure ( $\Delta P_f$ ). Note that the porosity ( $\phi$ ) effect is not explicitly stated here, but is included in the effective bulk modulus of the dry aggregate  $K$ .



## 2.2. $\beta_{\text{wet}_U}$ under Undrained Conditions

The term undrained refers to the boundary conditions in which there is no change in the pore fluid mass ( $dm_f=0$ ). Thus, for porous rocks, Skempton's coefficient ( $B$ ) is introduced. It is defined as the ratio of the pore fluid pressure change ( $\Delta P_f$ ) to the confining pressure change ( $\Delta P_c$ ) under undrained conditions, i.e.,  $B = (\Delta P_f / \Delta P_c)|_{dm_f=0}$  [Skempton, 1954; Green and Wang, 1986; Wang, 2000].  $B$  is also referred to as the undrained pore pressure coefficient. Thus, the changes in pore pressure and effective pressure within the skeletal framework of the porous rock are expressed as

$$\begin{cases} \Delta P_f = B \cdot \Delta P_c \\ \Delta P^{\text{eff}} = (1 - \alpha \cdot B) \cdot \Delta P_c \end{cases} \quad (9)$$

There is a classical thermoelastic relationship between the temperature change ( $\Delta T$ ) and the confining pressure change ( $\Delta P$ ) [Boley and Weiner, 1960; Wong *et al.*, 1987; Wong *et al.*, 1988; Turcotte and Schubert, 2014; Yang *et al.*, 2017]

$$\begin{cases} \Delta T = \beta \cdot \Delta P \\ \beta = \frac{\alpha_v}{\rho c_p} \cdot T_0 \end{cases}, \quad (10)$$

where  $\beta$  is the adiabatic pressure derivative of the temperature  $(\partial T / \partial P)_s$  at thermodynamic temperature  $T_0$ , and  $\alpha_v$  is the volumetric thermal expansion coefficient at  $T_0$ , which is three times the coefficient of linear thermal expansion (i.e.,  $\alpha_v = 3\alpha_l$ ) for isotropic materials.  $\rho c_p$  is the heat capacity per volume at constant pressure. Consequently, at the moment the confining pressure instantaneously changes, the temperature changes in the pore fluid ( $\Delta T_f$ ) and the skeletal framework of the porous rock ( $\Delta T_{\text{frm}}$ ) can be obtained from the following equations:

$$\begin{cases} \Delta T_{\text{frm}} = \beta_{\text{frm}} \cdot \Delta P^{\text{eff}} = (1 - \alpha \cdot B) \cdot \beta_{\text{frm}} \cdot \Delta P_c \\ \Delta T_f = \beta_f \cdot \Delta P_f = B \cdot \beta_f \cdot \Delta P_c \end{cases}, \quad (11)$$

where  $\beta_{\text{frm}}$  and  $\beta_f$  are defined as the adiabatic pressure derivatives of the temperature of the skeletal framework of the porous rock ( $\beta_{\text{frm}} = (\partial T_{\text{frm}} / \partial P_{\text{frm}})_s$ ) and the pore fluid ( $\beta_f = (\partial T_f / \partial P_f)_s$ ), respectively. Thus, the total heat energy change in the fluid-saturated porous rock per unit of bulk volume is

$$\Delta Q = \begin{cases} (\rho c)_{\text{frm}} \cdot \Delta T_{\text{frm}} + \phi \cdot (\rho c)_f \cdot \Delta T_f \\ \text{or} \\ [(1 - \alpha \cdot B) \cdot (\rho c)_{\text{frm}} \cdot \beta_{\text{frm}} + \phi \cdot B \cdot (\rho c)_f \cdot \beta_f] \cdot \Delta P_c \end{cases} \quad (12)$$

Equation (11) demonstrates that there must be a temperature difference between the skeletal framework and the pore fluid, i.e.,  $\Delta T_{\text{frm}} \neq \Delta T_f$ , at the moment at which the instantaneous change in the confining pressure occurs. In this study, we monitored the changes in the rock specimen temperature and the confining pressure using a data sampling interval of 1 s. For most of the porous rocks, the skeletal framework and the pore fluid (water) can reach thermal equilibrium by heat diffusion within 1 s of the instantaneous change in confining pressure since the sizes of the solid grains and the pores are limited. A detailed proof of the estimation of the characteristic distance using dimensional analysis and numerical simulation is provide in Section “Thermal equilibrium between the skeletal framework and the pore fluid” in Supporting Information. Consequently, Equations (1), (3), (4), and (12) can be combined to obtain the apparent temperature change of the fluid-saturated porous rock

$$\Delta T = \frac{\Delta Q}{(\rho c)} = \left\{ \frac{(1 - \alpha \cdot B) \cdot [(\rho c)_{\text{dry}} - \phi \cdot (\rho c)_a] \cdot \beta_{\text{frm}} + \phi \cdot B \cdot (\rho c)_f \cdot \beta_f}{(\rho c)_{\text{dry}} + \phi \cdot [(\rho c)_f - (\rho c)_a]} \right\} \cdot \Delta P_c. \quad (13)$$

Finally,  $\beta$  is calculated using the following equation:

$$\beta = \frac{\Delta T}{\Delta P_c} = \frac{(1 - \alpha \cdot B) \cdot [(\rho c)_{\text{dry}} - \phi \cdot (\rho c)_a] \cdot \beta_{\text{frm}} + \phi \cdot B \cdot (\rho c)_f \cdot \beta_f}{(\rho c)_{\text{dry}} + \phi \cdot [(\rho c)_f - (\rho c)_a]}. \quad (14)$$

The pores of dry porous rocks are filled with air, and thus,  $(\rho c)_f$  can be replaced with the volumetric heat capacity of air  $(\rho c)_a$ . In the experiments on the temperature response to pressure changes in dry rocks [Yang *et al.*, 2017], the change in the pore-air pressure in dry rocks was ignored because its coefficient of compressibility is so high ( $1/K_a \rightarrow \infty$ ). In this case, Skempton's coefficient  $B$  for dry porous rocks tends toward zero ( $B \rightarrow 0$ ) [Wang, 2000]. Consequently, the adiabatic pressure derivative of the temperature of dry porous rocks  $\beta_{dry}$  can be expressed as

$$\beta_{dry} = \frac{(1-\alpha \cdot B) \cdot [(\rho c)_{dry} - \phi \cdot (\rho c)_a] \cdot \beta_{frm} + \phi \cdot B \cdot (\rho c)_a \cdot \beta_a}{(\rho c)_{dry} + \phi \cdot [(\rho c)_a - (\rho c)_a]} = \frac{(\rho c)_{dry} - \phi \cdot (\rho c)_a}{(\rho c)_{dry}} \cdot \beta_{frm}. \quad (15)$$

In fact, under dry conditions,  $\beta_{dry}$  can be measured directly in laboratory experiments [Yang *et al.*, 2017]. Thus,  $\beta_{frm}$  can be calculated using the following equation:

$$\beta_{frm} = \frac{(\rho c)_{dry}}{(\rho c)_{dry} - \phi \cdot (\rho c)_a} \cdot \beta_{dry}. \quad (16)$$

Thus, Equation (14) can be re-written as

$$\beta = \frac{\phi \cdot (\rho c)_f \cdot \beta_f - \alpha \cdot (\rho c)_{dry} \cdot \beta_{dry}}{(\rho c)_{dry} + \phi \cdot [(\rho c)_f - (\rho c)_a]} \cdot B + \frac{(\rho c)_{dry} \cdot \beta_{dry}}{(\rho c)_{dry} + \phi \cdot [(\rho c)_f - (\rho c)_a]}. \quad (17)$$

For water-saturated porous rocks, the pores are filled with water, therefore

$$\begin{cases} (\rho c)_f = (\rho c)_w, \\ \beta_f = \beta_w \end{cases}, \quad (18)$$

where  $(\rho c)_w$  and  $\beta_w$  are the heat capacity per unit volume and the adiabatic pressure derivative of the temperature of water, respectively. Based on Equations (17) and (18), the adiabatic pressure derivative of the temperature of water-saturated porous rocks under undrained conditions ( $\beta_{wet\_U}$ ) can be expressed as

$$\beta_{wet\_U} = \frac{\phi \cdot (\rho c)_w \cdot \beta_w - \alpha \cdot (\rho c)_{dry} \cdot \beta_{dry}}{(\rho c)_{dry} + \phi \cdot [(\rho c)_w - (\rho c)_a]} \cdot B + \frac{(\rho c)_{dry} \cdot \beta_{dry}}{(\rho c)_{dry} + \phi \cdot [(\rho c)_w - (\rho c)_a]}. \quad (19)$$

Equation (19) shows that for porous rocks,  $\beta_{\text{wet\_U}}$  has a linear relationship with  $B$ , which depends on the physical properties of the porous rock, water, and air. These properties include the volumetric heat capacities  $(\rho c)_{\text{dry}}$ ,  $(\rho c)_{\text{w}}$ , and  $(\rho c)_{\text{a}}$ , the values of  $\beta_{\text{dry}}$  and  $\beta_{\text{w}}$ , and the porosity ( $\phi$ ).

### 2.3. $\beta_{\text{wet\_D}}$ under Drained Conditions

Relative to undrained conditions, the term drained refers to the boundary condition in which there is no change in the pore fluid pressure ( $\Delta P_{\text{f}} = 0$ ). Thus, in ideal drained conditions, for water-saturated porous rocks, the pore water pressure ( $P_{\text{w}}$ ) will remain constant even if the confining pressure changes. In such a case, the value of  $\Delta P_{\text{w}}$  is 0 (i.e.,  $\Delta P_{\text{w}} = \Delta P_{\text{f}} = 0$ ), and Equation (8) simplifies to

$$\Delta P^{\text{eff}} = \Delta P_{\text{c}}. \quad (20)$$

Therefore, we can express the temperature changes in the pore water ( $\Delta T_{\text{f}}$ ) and the skeletal framework of the porous rock ( $\Delta T_{\text{frm}}$ ) as

$$\begin{cases} \Delta T_{\text{frm}} = \beta_{\text{frm}} \cdot \Delta P^{\text{eff}} = \beta_{\text{frm}} \cdot \Delta P_{\text{c}} \\ \Delta T_{\text{w}} = \beta_{\text{w}} \cdot \Delta P_{\text{w}} = 0 \end{cases}. \quad (21)$$

Thus, the total heat energy change of the water-saturated porous rock per unit of bulk volume is

$$\Delta Q = (\rho c)_{\text{frm}} \cdot \beta_{\text{frm}} \cdot \Delta P_{\text{c}}. \quad (22)$$

To account for the macroscopic stress or pore pressure, *Biot* [1941] introduced the variation in water content  $\xi$ , which is defined as the variation in the pore water volume per unit volume of rock.

$$\begin{cases} \xi = \frac{\Delta P_{\text{c}}}{H} + \frac{\Delta P_{\text{w}}}{R} \\ \frac{1}{H} = \frac{1}{K} - \frac{1}{K_{\text{S}}} \\ \frac{1}{R} = \frac{1}{H} + \phi \cdot \left( \frac{1}{K_{\text{w}}} - \frac{1}{K_{\text{S}}} \right) \end{cases}, \quad (23)$$

where  $K_w$  is the bulk modulus of the pore water;  $1/H$  and  $1/R$  are the poroelastic expansion coefficient and the specific storage coefficient at constant stress, respectively [Rice and Cleary, 1976; Wang, 2000; Paterson and Wong, 2005]. A positive value of  $\xi$  indicates the removal of water.

Under drained conditions, there is no change in the pore water pressure ( $\Delta P_w = 0$ ). Hence, Equation (23) can be re-written as

$$\xi = \frac{1}{H} \cdot \Delta P_c = \left( \frac{1}{K} - \frac{1}{K_s} \right) \cdot \Delta P_c, \quad (24)$$

and the volumetric heat capacity of the water-saturated porous rock after loading/unloading under drained conditions can be expressed as

$$(\rho c) = (1 - \phi) \cdot (\rho c)_s + (\phi - \xi) \cdot (\rho c)_w. \quad (25)$$

Thus, the apparent temperature change of water-saturated rocks under drained conditions is

$$\Delta T = \frac{\Delta Q}{(\rho c)} = \frac{(\rho c)_{\text{frm}} \cdot \beta_{\text{frm}}}{(1 - \phi) \cdot (\rho c)_s + (\phi - \xi) \cdot (\rho c)_w} \cdot \Delta P_c. \quad (26)$$

Note that Equation (26) is also based on the fact that thermal equilibrium is reached between the solid grains and the pore water within 1 s after the instantaneous change in the confining pressure. Therefore, by combining Equations (3), (4), (16), and (20), the apparent adiabatic pressure derivative of the temperature of water-saturated porous rocks under drained conditions ( $\beta_{\text{wet}_D}$ ) can be expressed as

$$\begin{cases} \beta_{\text{wet}_D} = \frac{\Delta T}{\Delta P_c} = \frac{(\rho c)_{\text{dry}} \cdot \beta_{\text{dry}}}{(\rho c)_{\text{dry}} + \phi \cdot [(\rho c)_w - (\rho c)_a] - \xi \cdot (\rho c)_w} \\ \xi = \frac{1}{H} \cdot \Delta P_c \end{cases} \quad (27)$$

### 3. Calculated $\beta_{\text{wet\_U}}$ and $\beta_{\text{wet\_D}}$ of 15 Representative Rocks

In our previous work, we systematically measured not only the basic physical properties of 15 representative rocks, but also the adiabatic pressure derivatives of temperature of the 15 dry rocks ( $\beta_{\text{dry}}$ ) and water ( $\beta_{\text{w}}$ ) at room temperature (21°C–23°C) [Yang *et al.*, 2017]. The basic physical properties of the 15 rocks include the grain density ( $\rho_s$ ), the dry density ( $\rho_{\text{dry}}$ ), the porosity ( $\phi$ ), the volumetric heat capacity in the dry state  $(\rho c)_{\text{dry}}$ , and the bulk modulus ( $K$ ) in the dry state at 24°C–29°C and ~0.1 MPa. At 25°C and 0.1 MPa, the volumetric heat capacities of water  $((\rho c)_{\text{w}})$  and air  $((\rho c)_{\text{a}})$  are 4.169 MJ/(m<sup>3</sup>·K) [Lide, 2010] and 1.206×10<sup>-3</sup> MJ/(m<sup>3</sup>·K) [Yang and Tao, 2006], respectively.

Based on the above-determined basic physical properties of the 15 rocks, water, and air, the apparent adiabatic pressure derivatives of the temperature of the water-saturated porous rocks under undrained and drained conditions ( $\beta_{\text{wet\_U}}$  and  $\beta_{\text{wet\_D}}$ ) using Equations (19) and (27), respectively, can be calculated if the effective stress coefficient  $\alpha$ , Skempton's coefficient  $B$  and poroelastic expansion coefficient  $1/H$  are known. We did not measure  $\alpha$ ,  $B$  or  $1/H$  for each rock used in this study. Instead, we compiled 32 published laboratory poroelastic constants for compact and porous rocks (including granites, carbonates and sandstones) (Table 1). Figures 1a and 1b indicate that  $\alpha$  and  $1/H$  increase approximately linearly with porosity  $\phi$ . Most of the experimental results of  $\alpha$  and  $1/H$  are centrally distributed within the range delimited by Equations (28) and (29), respectively.

$$\text{FL01: } \alpha = (0.9794 \cdot \phi + 0.5507) \pm 0.15, R^2=0.50, \quad (28)$$

$$\text{FL02: } 1/H = (0.4988 \cdot \phi + 0.0015) \pm 0.06, R^2=0.65, \quad (29)$$

where the unit of  $1/H$  is GPa<sup>-1</sup>; and  $R^2$  is the coefficient of determination. Figure 1a also shows that  $\alpha$  usually ranges from  $\phi$  to 1 (i.e.,  $\phi \leq \alpha \leq 1$ ) [Berryman, 1992; Wang, 2000]. From Equation (23), we know that  $1/H$  must be more than 0 since the

drained bulk modulus  $K$  is always less than theunjacketed modulus  $K_s$ , i.e.,  $1/H = (1/K - 1/K_s) \geq 0$ . Table 2 lists the estimated ranges of  $\alpha$  and  $1/H$  for the 15 rocks obtained from Equations (28) and (29). Even though Skempton's coefficient  $B$  tends to decrease with porosity  $\phi$ , they are not directly related (Figure 1c). However, the value of  $B$  must be between 0 and 1. In this study, the change in confining pressure  $\Delta P_c$  is between 0 and 15 MPa during the loading/unloading processes, i.e.,  $0 \leq |\Delta P_c| \leq 15$  MPa (Table 3).

Consequently, the ranges of  $\beta_{\text{wet}_U}$  and  $\beta_{\text{wet}_D}$  for the 15 rocks can be calculated using Equations (19) and (27) since the ranges of  $\alpha$ ,  $B$ ,  $1/H$  and  $\Delta P_c$  are limited. We list the results in Table 2, and show the calculated  $\beta_{\text{wet}_U}$  with given  $\alpha$  and  $B$  in Figure 2.

## **4. Experimental Methods and Results**

### **4.1. Rock Samples**

To verify the above theoretical analysis of the temperature response of fluid-saturated porous rocks to changes in stress, we systematically measured the  $\beta_{\text{wet}}$  of a low porosity ( $\phi = 0.003$ ) limestone (sample L27) and a medium porosity ( $\phi = 0.102$ ) sandstone (sample RJS). Samples L27 and RJS are from the Longmenshan Fault Zone in Sichuan, China, and the Rajasthan, India, respectively. Limestone L27 and sandstone RJS represent a compact rock and a porous rock, respectively. The two rock samples were cut into cylindrical specimens. The diameter ( $D_r$ ) and length ( $L$ ) of the rock specimens are both 50 mm (Figures 3 and 4). Their basic properties were measured at 24°C–29°C and ~0.1 MPa [Yang *et al.*, 2017]. The measured properties are listed in Table 2.

## **4.2. Measurement System and Experimental Procedure**

In this study, it was necessary to measure the values of  $\beta_{\text{wet\_U}}$  and  $\beta_{\text{wet\_D}}$ , which required improvements to the hydrostatic compression system used to measure the adiabatic pressure derivative of the temperature of dry rocks ( $\beta_{\text{dry}}$ ) [Yang *et al.*, 2017]. The improved hydrostatic compression system (Figure S1) and experimental procedure are similar to that used to measure  $\beta_{\text{dry}}$ , except for the inner structures related to the sample assembly. Thus, in this section, only the inner structures of the sample assembly (Figures 3 and 4) are described. Detailed descriptions of the measurement system and experimental procedure are provided in the Supporting Information.

To monitor the temperature response of the rock specimen, a small hole was drilled in the cylindrical rock sample center to allow for the installation of a temperature sensor. In this study, the diameter ( $D_h$ ) and depth ( $H$ ) of the central hole were 2.80 mm and 26.00 mm, respectively (Figures 3 and 4). The apparatus setup shown in Figure 3 was adapted for undrained conditions by inserting a steel tube into the central hole with a 0.15 mm gap between the walls of the steel tube and the hole. In addition, the apparatus setup shown in Figure 4 was used for drained conditions because there is nothing in the central hole except for the miniature temperature sensor T01. In reality, the cavity in the center of the rock sample was not an infinite reservoir that would allow for the pore pressure to drop to zero under ideal drained conditions, nor it was small enough or well-sealed enough to perfectly simulate ideal undrained conditions during the rapid loading/unloading processes. Therefore, in the experiments conducted in this study, we were able to closely approach the undrained/draind conditions, but we could not achieve the ideal undrained/draind conditions. Thus, the experiments conducted in this study can be considered to have been carried out under quasi-undrained/quasi-draind conditions.



### **4.3. Experimental Data Analysis and Results**

A set of loading/unloading tests was carried out on water-saturated sandstone RJS and water-saturated limestone L27 (Table 3). We denote these tests as RJS(W)-13, -14, and -15 under quasi-undrained conditions (Figure 5), RJS(W)-16, -17, and -18 (Figure 6) and L27(W)-01, -02, and -03 (Figure 7) under quasi-drained conditions. All experimental data are not only listed in Table S1 in Supporting Information, but also stored and provided in a data repository (<http://doi.org/10.5281/zenodo.4242969>). The temperature records demonstrate that the temperature response characteristics in the center of the rock specimens differed under quasi-undrained conditions (Figure 5) and quasi-drained (Figures 6 and 7) conditions. Consequently, in this section, the temperature responses during loading/unloading under quasi-undrained and quasi-drained conditions are analyzed in detail, respectively.

#### **4.3.1. Under Quasi-Undrained Conditions**

Taking test RJS(W)-13 as an example, during the period of temperature equilibration, the confining pressure in Vessel B was maintained at 3.39 MPa, and the system's temperature tended to equilibrate at 22.725°C (Table 3). When valve V03 was rapidly opened manually (i.e.,  $Time = 0$  s in Figure 5), the confining pressure in Vessel B dropped from 3.39 MPa to atmospheric pressure ( $\sim 0.1$  MPa) within 1–2 s. Simultaneously, the temperature in the rock specimen center and the oil dropped rapidly.

The reason for the temperature change in the rock sample center ( $\Delta T_{01}$ ) during unloading (Figure 5a1) is not entirely clear because the temperature change in oil ( $\Delta T_{03}$ ) was much larger during the same period. However,  $\Delta T_{01}$  is the actual change in the rock sample's temperature that is required. Therefore, only the changes in the

1 temperature in the rock specimen center and the pressure in Vessel B are shown in  
2 Figure 5a2. This illustrates that the temperature in the rock specimen decreased  
3 sharply to the lowest peak (-76 mK) during the first 3 s after the rapid unloading,  
4 and then, it increased during 3–13 s. The temperature peak (-76 mK) was induced  
5 by the temperature response of the water around the steel tube to the instantaneous  
6 confining pressure drop because the  $\beta$  of the water ( $\beta_w$ : ~17.0–26.0 mK/MPa, Table  
7 3) is much greater than the  $\beta$  of dry rocks ( $\beta_{dry}$ : ~1.5–6.2 mK/MPa) at room  
8 temperature [Yang *et al.*, 2017]. This is discussed further in Section 5.1.

9 During the next several seconds (13–20 s), the central temperature remained nearly  
10 constant, much like the temperature steps in dry rock experiments conducted in a  
11 previous study [Yang *et al.*, 2017]. This means that, during the first ~20 s after rapid  
12 unloading, the central temperature of the rock specimen was only induced by the  
13 pressure change, but evidently not affected by the oil temperature change. Then, the  
14 temperature decreased gradually again because the specimen's center was affected  
15 by heat conduction due to the temperature difference between the specimen and the  
16 oil after the rapid unloading (Figure 5a1). Similar characteristics of temperature  
17 response are exhibited in tests RJS(W)-14 and -15 (Figures 5b2 and 5c2).

18 Consequently, the temperature changes ( $\Delta T$ ) indicated by the temperature steps  
19 ( $t=13$ –20 s) from tests RJS(W)-13, -14, and -15 were obtained. Then, the values of  
20  $\beta_{wet\_Meas}$  for sample RJS were calculated from the values of  $\Delta T/\Delta P$ . The results show  
21 that the  $\beta_{wet\_Meas}$  of sample RJS are ~4.61–6.68 mK/MPa under quasi-undrained  
22 conditions (Figure 5, Table 3). These experimental results are larger than the  
23 calculated results (3.78–5.37 mK/MPa) of the water-saturated Rajasthan sandstone  
24 (Figure 2k, Table 2). The comparison is discussed further in Section 5.3.

#### 4.3.2. Under Quasi-Drained Conditions

Under quasi-drained conditions, there were no sharp temperature peaks in the specimen's center after rapid loading/unloading (Figures 6 and 7). The characteristics of the temperature responses differ from those under quasi-undrained conditions (Figure 5) but are similar to those of the dry rock experiments [Yang *et al.*, 2017].

Here, we also take test L27(W)-01 as an example. In this test, the system temperature tended to equilibrate at 23.442°C (Table 3) more than 4 hours after placing the specimen in Vessel B. During this period, the confining pressure in Vessel B was maintained at atmospheric pressure. In Figure 7a, at  $t = 0$  s, valve V02 was rapidly opened manually and valve V03 was kept closed. The confining pressure in Vessel B increased to ~6.83 MPa within 1–2 s (Figure 7a). It is worth noting that the temperature in the hole center increased gradually during the first ~7 s after rapid loading, after which it remained nearly constant from  $t = 7$  s to  $t = 18$  s. Then, it increased again because of heat conduction from the oil (Figure 7a). Figures 7b and 7c show similar temperature responses during the rapid unloading using the same procedure and operation as those used in experiments conducted on dry rocks in our previous study [Yang *et al.*, 2017]. The temperature steps ( $t=7$ –18 s) reveal that the central temperature of sample L27 was only caused by the pressure change, but not influenced by the oil temperature change during the first ~18 s. Distinct temperature steps also occurred in tests L27(W)-02 and -03 (Figures 7b2 and 7c2) and tests RJS(W)-16, -17, and -18 (Figures 6a2, 6b2 and 6c2) after rapid loading/unloading.

Consequently, the  $\beta_{\text{wet\_Meas}}$  values of the water-saturated limestone and Rajasthan sandstone under quasi-drained conditions were determined from the values of  $\Delta T/\Delta P$  based on the temperature steps observed in tests L27(W)-01, -02, and -03 ( $t = 7$ –18 s) and tests RJS(W)-16, -17, and -18 ( $t = 8$ –19 s), respectively. The measured

$\beta_{\text{wet\_Meas}}$  values of samples L27 and RJS are 0.92–1.50 mK/MPa and 3.57–3.61 mK/MPa, respectively (Figures 6 and 7, Tables 2 and 3), which are less than the calculated  $\beta_{\text{wet\_D}}$  values (L27: 1.52–1.55 mK/MPa; RJS: 3.78–3.91 mK/MPa). A detailed comparison between the measured and calculated results is presented in Section 5.3.

## **5. Discussion**

### **5.1. Temperature Response Characteristics under Quasi-Undrained and Quasi-Drained Conditions**

Figures 5 and 6 (under undrained and drained conditions, respectively) show significantly different temperature response characteristics for the water-saturated sandstone RJS(W) after rapid loading/unloading, especially during the first ~10 s. Sharp temperature peaks occurred in tests RJS(W)-13, -14, and -15 under quasi-undrained condition, but did not occur in tests RJS(W)-16, -17 and -18 under quasi-drained condition.

As described in Section 4.2, in order to as closely as possible simulate drained conditions, only the miniature temperature sensor T01 was placed in the central hole (Figure 4). In this case, in tests RJS(W)-16, -17, and -18, the central hole, which had with a diameter of 2.80 mm, could not be filled fully by the pore water from the pores in the area around the central hole after the rapid loading/unloading. Consequently, during the first few seconds after the instant loading/unloading, there was no obvious change in the pore pressure in the area around the central hole, and no temperature peaks were recorded (Figure 6). Of course, there must be a change in pore pressure throughout the rock sample except for in the area directly around the hole.

In tests RJS(W)-13, -14, and -15 (Figure 5), to achieve undrained conditions, a steel tube with temperature sensor T01 was inserted in the central hole in the rock specimen (Figure 3). Between the steel tube and the hole wall, there was a very small 0.15 mm gap, which was easier to fill fully with the pore water from the pores in the area around the hole after rapid loading. Then, the water in the gap underwent compression/decompression during the loading/unloading processes, resulting in an instantaneous increase in temperature. This is the reason for the sharp temperature peaks during the first 3–4 s after rapid loading/unloading in tests RJS(W)-13, -14, and -15 (Figure 5) since the  $\beta$  value of water ( $\beta_w$ ) reaches 17.76 mK/MPa at  $\sim 21^\circ\text{C}$  and 26.03 mK/MPa at  $\sim 31^\circ\text{C}$  (Table 3), which is much higher than the  $\beta$  value of dry rock ( $\beta_{\text{dry}}$ :  $\sim 1.5\text{--}6.2$  mK/MPa) [Yang *et al.*, 2017].

## **5.2. Ranges of $\beta_{\text{wet}}$ under Undrained and Drained Conditions**

In Section 2, the adiabatic pressure derivatives of the temperature of the water-saturated porous rocks under both undrained ( $\beta_{\text{wet}_U}$ ) and drained ( $\beta_{\text{wet}_D}$ ) conditions were deduced. The quantitative equation for  $\beta_{\text{wet}_U}$  and  $\beta_{\text{wet}_D}$  were also derived based on the basic physical properties of dry rocks, water, and air, as shown in Equations (19) and (27). However, it is difficult to obtain the values of  $\alpha$  and  $B$  in Equation (19) and  $1/H$  in Equation (27) during actual geological processes, i.e., the actual values of  $\beta_{\text{wet}_U}$  and  $\beta_{\text{wet}_D}$  cannot be calculated. However, it is still useful for understanding the temperature responses in various geological phenomena that induce changes in stress. Therefore, in this section, the ranges of  $\beta_{\text{wet}_U}$  and  $\beta_{\text{wet}_D}$  for all 15 rock samples are analyzed based on Equations (19) and (27). In addition, the basic physical properties of the rock samples (Table 2), water, and air are described in Section 3.

For undrained conditions, Figure 2 shows that  $\beta_{\text{wet}_U}$  decreases with  $B$  when  $\phi < 0.05$ , but increases with  $B$  when  $\phi > 0.05$ . This implies that  $\beta_{\text{wet}_U}$  will reach a

maximum/minimum when  $B$  is 0 or 1. Therefore, according to Equation (19), the range of  $\beta_{\text{wet\_U}}$  can be obtained from the following equations.

If  $\phi < 0.05$ ,

$$\frac{\phi \cdot (\rho c)_w \cdot \beta_w + (1 - \alpha) \cdot (\rho c)_{\text{dry}} \cdot \beta_{\text{dry}}}{(\rho c)_{\text{dry}} + \phi \cdot [(\rho c)_w - (\rho c)_a]} \leq \beta_{\text{wet\_U}} \leq \frac{(\rho c)_{\text{dry}} \cdot \beta_{\text{dry}}}{(\rho c)_{\text{dry}} + \phi \cdot [(\rho c)_w - (\rho c)_a]}, \quad (30)$$

and if  $\phi > 0.05$ ,

$$\frac{(\rho c)_{\text{dry}} \cdot \beta_{\text{dry}}}{(\rho c)_{\text{dry}} + \phi \cdot [(\rho c)_w - (\rho c)_a]} \leq \beta_{\text{wet\_U}} \leq \frac{\phi \cdot (\rho c)_w \cdot \beta_w + (1 - \alpha) \cdot (\rho c)_{\text{dry}} \cdot \beta_{\text{dry}}}{(\rho c)_{\text{dry}} + \phi \cdot [(\rho c)_w - (\rho c)_a]}. \quad (31)$$

For drained conditions, Equation (27) illustrates that  $\beta_{\text{wet\_D}}$  decreases nonlinearly with increasing water content  $\zeta$  (i.e.,  $\Delta P_c/H$ ). During the drained loading process, the water content decreases with increasing confining pressure (i.e.,  $\Delta P_c > 0$ ). Thus, the range of  $\beta_{\text{wet\_D}}$  can be obtained from the following equation:

$$\frac{(\rho c)_{\text{dry}} \cdot \beta_{\text{dry}}}{(\rho c)_{\text{dry}} + \phi \cdot [(\rho c)_w - (\rho c)_a]} \leq \beta_{\text{wet\_D}} \leq \frac{(\rho c)_{\text{dry}} \cdot \beta_{\text{dry}}}{(\rho c)_{\text{dry}} + \phi \cdot [(\rho c)_w - (\rho c)_a] - (\rho c)_w \cdot \Delta P_c/H}. \quad (32)$$

Conversely, during the drained unloading process, some of the water is absorbed into the rock pores because the pore space increases when the confining pressure decreases. The most extreme situation occurs when the confining pressure tends towards the atmospheric pressure ( $\sim 0.1$  MPa), resulting in the water content of the porous rocks reaching the maximum value. The volumetric heat capacity of the water-saturated rocks (the denominator term in Equation (27)) will be up to the maximum value. Hence,  $\beta_{\text{wet\_D}}$  will reach the minimum value. The porosities of all of the rocks were measured in our previous article [Yang *et al.*, 2017], implying that the left term in Equation (32) is also the lower limit of  $\beta_{\text{wet\_D}}$  during drained unloading.

From the above analysis, we obtained the following lower/upper limits for  $\beta_{\text{wet\_U}}$  and  $\beta_{\text{wet\_D}}$ .

1 If  $\phi < 0.05$ ,

$$2 \quad \begin{cases} \beta_{\text{wet\_U\_Min}} = \frac{\phi \cdot (\rho c)_w \cdot \beta_w + (1-\alpha) \cdot (\rho c)_{\text{dry}} \cdot \beta_{\text{dry}}}{(\rho c)_{\text{dry}} + \phi \cdot [(\rho c)_w - (\rho c)_a]} \\ \beta_{\text{wet\_U\_Max}} = \beta_{\text{wet\_D\_Min}} = \frac{(\rho c)_{\text{dry}} \cdot \beta_{\text{dry}}}{(\rho c)_{\text{dry}} + \phi \cdot [(\rho c)_w - (\rho c)_a]} < \beta_{\text{dry}}, \\ \beta_{\text{wet\_D\_Max}} = \frac{(\rho c)_{\text{dry}} \cdot \beta_{\text{dry}}}{(\rho c)_{\text{dry}} + \phi \cdot [(\rho c)_w - (\rho c)_a] - (\rho c)_w \cdot \Delta P_c / H}, \Delta P_c > 0 \end{cases} \quad (33)$$

3 and if  $\phi > 0.05$ ,

$$4 \quad \begin{cases} \beta_{\text{wet\_U\_Max}} = \frac{\phi \cdot (\rho c)_w \cdot \beta_w + (1-\alpha) \cdot (\rho c)_{\text{dry}} \cdot \beta_{\text{dry}}}{(\rho c)_{\text{dry}} + \phi \cdot [(\rho c)_w - (\rho c)_a]} \\ \beta_{\text{wet\_U\_Min}} = \beta_{\text{wet\_D\_Min}} = \frac{(\rho c)_{\text{dry}} \cdot \beta_{\text{dry}}}{(\rho c)_{\text{dry}} + \phi \cdot [(\rho c)_w - (\rho c)_a]} \\ \beta_{\text{wet\_D\_Max}} = \frac{(\rho c)_{\text{dry}} \cdot \beta_{\text{dry}}}{(\rho c)_{\text{dry}} + \phi \cdot [(\rho c)_w - (\rho c)_a] - (\rho c)_w \cdot \Delta P_c / H}, \Delta P_c > 0 \end{cases} \quad (34)$$

5 In fact, in Section 3, we calculated the lower and upper limits of  $\beta_{\text{wet}}$  for all of the 15  
6 porous rocks used in this study (Table 2). Figure 8 illustrates the calculated ranges  
7 of  $\beta_{\text{wet}}$  under both undrained and drained conditions. Both of the calculated results  
8 and Equations (33) and (34) show that 1) when the porosity is within 0.05, the upper  
9 limit of  $\beta_{\text{wet\_U}}$  equates to the lower limit of  $\beta_{\text{wet\_D}}$ , and both of them are less than  $\beta_{\text{dry}}$   
10 (Figure 8a); and 2) when the porosity exceeds 0.05, the lower limits of  $\beta_{\text{wet\_U}}$  and  
11  $\beta_{\text{wet\_D}}$  are the same, which indicate that there is no change in pore-water pressure  
12 (i.e.,  $B = 0$ ) under undrained conditions, and no change in the pore-water content  
13 (i.e.,  $\xi = 0$ ) under drained conditions. In addition, the upper limits of  $\beta_{\text{wet\_U}}$  and  $\beta_{\text{wet\_D}}$   
14 indicate that the pore pressure change reaches a maximum, which equates to the  
15 change in confining pressure (i.e.,  $B = 1$ ), under undrained conditions, while part of  
16 the pore water has drained from the rock pores (i.e.,  $\xi = \Delta P_c / H$ ) under the drained  
17 conditions (Figure 8b). Figure 8 also clearly shows the following. 1) The range of  
18  $\beta_{\text{wet\_U}}$  contains the range of  $\beta_{\text{wet\_D}}$ , which is very narrow. This indicates that in most  
19 cases, it is sufficient only to analyze the lower and upper limits of  $\beta_{\text{wet}}$  under

undrained conditions because most geological processes occur in between the undrained and drained conditions. 2) The range of  $\beta_{\text{wet\_U}}$  becomes wider with the increase of porosity, especially when the porosity is greater than 0.05 (i.e.,  $\phi > 0.05$ ) (Figure 8b).

Also, the experimental results show that the values of  $B$  are typically between 0.5 and 1.0 for water-saturated rocks [Wang, 2000]; can be greater, e.g., 0.87–0.95 range for the Berea sandstone ( $\phi \approx 0.20$ ), when the confining pressure is 40–60 MPa [Green and Wang, 1986]; can reach 0.97–0.99 for natural sandstone ( $\phi \approx 0.15$ ) when the differential pressure is about 1 MPa [Berge *et al.*, 1993]; and can approach 1.0 for water-saturated soil [Wang, 2000]. In this study, the minimum values of  $\beta_{\text{wet\_U}}$  for all of the 15 rocks were estimated when  $B = 0.5$  using the same method as in Section 3. The results of  $\beta_{\text{wet\_U\_Min}}(B=0.5)$  are shown in Figure 8 and are reported in Table 2. This indicates the following. 1) The values of  $\beta_{\text{wet\_U}}$  will have a narrower range because  $B$  is typically in the 0.5–1.0 range under natural conditions, rather than 0–1. 2) When  $B = 0.5$  and porosity is  $\phi > 0.05$ , the minimum values of  $\beta_{\text{wet\_U}}$  are slightly lower than the  $\beta$  of dry rocks ( $\beta_{\text{dry}}$ ), but they are very close to  $\beta_{\text{dry}}$  (Figure 8b). In other words, in most cases, the temperature response of rocks with a porosity of  $\phi > 0.05$  under water-saturated and undrained conditions is greater than that under dry conditions. This is much more conducive to and important for understanding temperature response characteristics in nature, for example, the temperature anomalies in boreholes drilled through seismically active faults after the Chi-Chi Earthquake, the Wenchuan Earthquake, and the Tohoku Earthquake [Kano *et al.*, 2006; Li *et al.*, 2013; Li *et al.*, 2015; Fulton *et al.*, 2013].



### 5.3. Comparison between the Measured and Calculated $\beta_{\text{wet}}$ Values

In Section 4, we systematically measured the  $\beta_{\text{wet}}$  of water-saturated limestone (L27,  $\phi = 0.003$ ) and sandstone (RJS,  $\phi = 0.102$ ). However, the measured  $\beta_{\text{wet}}$  of samples L27 and RJS were not entirely within the calculated ranges (Figure 8).

For the sandstone (RJS), the measured  $\beta_{\text{wet\_Meas(RJS)}}$  under quasi-undrained conditions was 4.61–6.68 mK/MPa (Figure 5, Table 3), which is broadly larger than the calculated results under undrained conditions ( $\beta_{\text{wet\_U(RJS)}} = 4.01\text{--}5.37$  mK/MPa, even if  $B = 0.5\text{--}1.0$ ) (Table 2). However, the measured  $\beta_{\text{wet\_Meas(RJS)}}$  (3.57–3.61 mK/MPa) under quasi-drained conditions (Figure 6, Table 3) was lower than the calculated results for drained conditions ( $\beta_{\text{wet\_D(RJS)}} = 3.78\text{--}3.91$  mK/MPa) (Table 2). As was mentioned in Section 4.2, we drilled a hole in the center of the rock samples ( $D_{\text{h}} = 2.8$  mm) and inserted a steel tube ( $D_{\text{so}} = 2.5$  mm) containing temperature sensor T01 to as closely as possible approximate undrained conditions (Figure 3). To a large degree, the effective porosity of the rock samples, especially in the area around the steel tube, would significantly increase since there was a 0.15 mm gap between the walls of the steel tube and the hole. In the area around the steel tube (even if we cannot define the specific scope), if the effective porosity increases to 0.15 (denoted by  $\phi'_{\text{RJS}} = 0.15$ ), then we can estimate the ranges of  $\beta_{\text{wet\_U(RJS)}}$  and  $\beta_{\text{wet\_D(RJS)}}$  using Equations (19) and (27), respectively, using the same method (see Section 3). The estimated results are  $\beta_{\text{wet\_U(RJS)}} = 4.34\text{--}6.25$  mK/MPa when  $B$  ranges from 0.5 to 1.0, and  $\beta_{\text{wet\_D(RJS)}} = 3.46\text{--}3.59$  mK/MPa. In this case, the measured  $\beta_{\text{wet\_Meas(RJS)}}$  is in good agreement with the theoretical estimates.

For the limestone (L27), the effective porosity also increased after drilling a 2.8 mm diameter hole. Using the same method, the ranges of  $\beta_{\text{wet\_U(L27)}}$  and  $\beta_{\text{wet\_D(L27)}}$  can be estimated if the effective porosity reached 0.01 (denoted by  $\phi'_{\text{L27}} = 0.01$ ) in the area around the hole. The range of  $\beta_{\text{wet\_U(L27)}}$  was estimated to be 0.76–1.50 mK/MPa

when  $B$  is 0–1. In addition, the range of  $\beta_{\text{wet\_D(L27)}}$  was estimated to be 1.50–1.53 mK/MPa. The measured results for limestone L27 ( $\beta_{\text{wet\_Meas(L27)}} = 0.92\text{--}1.50$  mK/MPa, Figure 7 and Table 3) are in the range of  $\beta_{\text{wet\_U(L27)}}$  (0.76–1.50 mK/MPa). This implies that the temperature response of the very low porosity rocks occurred under almost ideal undrained condition during the rapid loading/unloading processes, even the rock sample contained a central hole, which would be expected to result in drained conditions (Figure 4).

The above analysis indicates that the measured results are consistent with the calculated ranges for both the undrained and drained conditions. Consequently, both the theoretical analyses and the measurement results in this study are correct and reliable.

## **6. Conclusions**

Determining the characteristics of the temperature responses of water-saturated rocks to stress changes is key for comprehending the temperature anomalies in the crust, particularly because most of the porous rocks in the upper crust are saturated with groundwater. Consequently, the adiabatic pressure derivative of the temperature of water-saturated rocks was established for both undrained ( $\beta_{\text{wet\_U}}$ ) and drained ( $\beta_{\text{wet\_D}}$ ) conditions. The theoretical derivation results show that  $\beta_{\text{wet\_U}}$  is linearly correlated with Skempton's coefficient ( $B$ ) and that  $\beta_{\text{wet\_D}}$  increases nonlinearly with increasing pore water volume per unit volume of rock ( $\xi$ ). Both  $\beta_{\text{wet\_U}}$  and  $\beta_{\text{wet\_D}}$  depend on the adiabatic pressure derivatives of the temperature of dry rocks and water, the volumetric heat capacities of dry rocks, water, and air, and rock's porosity. Based on the theoretical analysis,  $\beta_{\text{wet\_U}}$  and  $\beta_{\text{wet\_D}}$  were calculated for 15 rock samples. The calculated results indicate that the range of  $\beta_{\text{wet\_U}}$  becomes wider with increasing porosity, especially when the porosity ( $\phi$ ) is greater than 0.05; while  $\beta_{\text{wet\_U}}$  increases with increasing  $B$  when  $\phi > 0.05$ , but decreases with increasing

1  $B$  when  $\phi < 0.05$ . For each rock, the range of  $\beta_{\text{wet\_D}}$  is very narrow and is within the  
2 range of  $\beta_{\text{wet\_U}}$ . Thus, it is sufficient only to analyze the range of  $\beta_{\text{wet}}$  under undrained  
3 conditions since most geological processes occur between undrained and drained  
4 conditions.

5 Several experiments were carried out on water-saturated sandstone (RJS) and  
6 limestone (L27) using an improved hydrostatic compression system. The  
7 experiments show that under quasi-undrained conditions, the measured  $\beta_{\text{wet\_Meas}}$  of  
8 sample RJS is 6.04–6.68 mK/MPa, which is broadly larger than the calculated  
9  $\beta_{\text{wet\_U(RJS)}}$  (4.01–5.37 mK/MPa) under undrained conditions, even when  $B$  was set to  
10 0.5–1.0. However, under quasi-drained conditions, the measured  $\beta_{\text{wet\_Meas(RJS)}}$  (3.57–  
11 3.61 mK/MPa) (Figure 6, Table 3) is lower than the calculated results under drained  
12 conditions ( $\beta_{\text{wet\_D(RJS)}} = 3.78\text{--}3.91$  mK/MPa). The measured  $\beta_{\text{wet\_Meas(RJS)}}$  is in good  
13 agreement with the theoretical estimates after considering the increase in effective  
14 porosity caused by drilling a hole in the sample. The measured results for limestone  
15 L27,  $\beta_{\text{wet\_Meas(L27)}}$  (0.92–1.50 mK/MPa), is in the range of the calculated  $\beta_{\text{wet\_U(L27)}}$   
16 (0.76–1.50 mK/MPa) after taking into account the increase in the effective porosity  
17 caused by drilling a hole in the sample. This implies that the temperature responses  
18 of the very low porosity rocks occurred under almost ideal undrained condition  
19 during loading/unloading processes. Overall, the measured results are consistent  
20 with the calculated results for both undrained and drained conditions, indicating that  
21 both the theoretical and experimental analyses are reliable.

22 Typically,  $B$  is in the 0.5–1.0 range for water-saturated rocks, rather than in the 0–1  
23 range that occurs in natural conditions, implying that  $\beta_{\text{wet\_U}}$  will be within a  
24 calculable and narrow range. In most cases, the temperature response of rocks with  
25 a porosity of  $\phi > 0.05$  is greater under water-saturated and undrained conditions than  
26 that under dry conditions. This study improves our understanding of and preparation

for co-seismic temperature responses, as there must be co-seismic stress changes in the future, such as the temperature anomalies observed in boreholes drilled through seismically active faults after the Chi-Chi, Wenchuan, and Tohoku earthquakes.

#### **Data Availability Statement**

Datasets for this research are available in *Yang et al.* [2020] and have been deposited in Zenodo (<http://doi.org/10.5281/zenodo.4242969>). The first dataset (Table S1) includes the temperature response of water-saturated porous Rajasthan sandstone (RJS) (Figures 5-6) and compact Longmenshan limestone (L27) (Figure 7) and to changes in confining pressure under drained/undrained conditions. The second dataset (Table S2) includes the thermal properties of rock-forming minerals and estimations of thermal characteristic time/distance. The third dataset includes the internal temperature evolution of the water-saturated sample within 1 s after instantaneous loading in models M-01 (Movie S1), M-02 (Movie S2) and M03 (Movie S3), in which the thermal properties of the solid grains are set to be that of gypsum, average values of the main rock-minerals and  $\alpha$ -quartz, respectively. Meanwhile, all study data are included in the article and Supporting Information Appendix.

#### **Acknowledgements**

We thank Chi-Yuen Wang for helpful discussions, Zhigang Zhang for partial technical support to measure the temperature response of tap water at room temperature, and Takehiro Hirose and Huan Wang for providing the original photomicrographs of thin sections of Rajasthan sandstone from India and cataclasite and fault breccia from the Longmenshan Fault Zone, respectively. We really thank the two Reviewers, Associate Editor and Editor Douglas Schmitt for careful reading and constructive comments which help us to improve this manuscript. This work was supported by the Key Special Project for Introduced Talents Team of Southern

Marine Science and Engineering Guangdong Laboratory (Guangzhou) (GML2019ZD0104), the National Natural Science Foundation of China (41874099, 41474065 and 41376061) and the Instrument Developing Project of the Chinese Academy of Sciences (YZ201136). W. Lin acknowledges the supports of the Japan Society for the Promotion of Science (JSPS KAKENHI Grant Number JP16H04065).

## References

- Arai, K., et al. (2013), Tsunami-generated turbidity current of the 2011 Tohoku-Oki earthquake, *Geology*, 41(11), 1195-1198, doi:10.1130/G34777.1.
- Berge, P. A., H. F. Wang, and B. P. Bonner (1993), Pore pressure buildup coefficient in synthetic and natural sandstones, *International Journal of Rock Mechanics and Mining Sciences & Geomechanics Abstracts*, 30(7), 1135-1141, doi:http://dx.doi.org/10.1016/0148-9062(93)90083-P.
- Berryman, J. G. (1992), Exact effective-stress rules in rock mechanics, *Physical Review A*, 46(6), 3307-3311, doi:10.1103/PhysRevA.46.3307.
- Biot, M. A. (1941), General Theory of Three - Dimensional Consolidation, *Journal of Applied Physics*, 12(2), 155-164, doi:10.1063/1.1712886.
- Biot, M. A. (1956), Thermoelasticity and Irreversible Thermodynamics, *Journal of Applied Physics*, 27(3), 240-253, doi:10.1063/1.1722351.
- Boley, B. A., and J. H. Weiner (1960), *Theory of thermal stresses*, Wiley, New York.
- Bourbié, T., O. Coussy, and B. Zinszer (1987), *Acoustics of porous media*, Editions Technip.
- Carlson D.E. (1973) Linear Thermoelasticity. In: Truesdell C. (eds) *Linear Theories of Elasticity and Thermoelasticity*. Springer, Berlin, Heidelberg. [https://doi.org/10.1007/978-3-662-39776-3\\_2](https://doi.org/10.1007/978-3-662-39776-3_2)
- Carreno, E., R. Capote, A. Yague, J. Tordesillas, M. Lopez, J. Ardizzone, A. Suarez, A. Lzquierdo, M. Tsige, and J. Martinez (2001), Observations of thermal anomaly associated to seismic activity from remote sensing, General Assembly of European Seismology Commission, Portugal, 265-269.
- Cheng, A. H.-D. (2016), *Poroelasticity*, Springer International Publishing.
- Chen, S., L. Liu, P. Liu, J. Ma, and G. Chen (2009), Theoretical and experimental study on relationship between stress-strain and temperature variation, *Science in China Series D: Earth Sciences*, 52(11), 1825-1834.
- Chen, S., P. Liu, Y. Guo, L. Liu, and J. Ma (2015), An experiment on temperature variations in sandstone during biaxial loading, *Physics and Chemistry of the Earth*,

- 1 Parts A/B/C, 85–86, 3-8, doi:<http://dx.doi.org/10.1016/j.pce.2014.10.006>.
- 2 Chen, S., P. Liu, L. Liu, and J. Ma (2013), A phenomenon of ground temperature  
3 change prior to Lushan Earthquake observed in Kangding, *Seismology and*  
4 *Geology*, 35(3), 634-640.
- 5 Chen, S., P. Liu, L. Liu, and J. Ma (2016), Bedrock temperature as a potential method  
6 for monitoring change in crustal stress: Theory, in situ measurement, and a case  
7 history, *Journal of Asian Earth Sciences*, 123, 22-33,  
8 doi:<http://dx.doi.org/10.1016/j.jseaes.2016.03.018>.
- 9 Chen, S., P. Liu, Y. Guo, L. Liu, and J. Ma (2019), Co-Seismic Response of Bedrock  
10 Temperature to the Ms6.3 Kangding Earthquake on 22 November 2014 in Sichuan,  
11 China, *Pure and Applied Geophysics*, 176(1), 97-111, doi:10.1007/s00024-018-  
12 1933-7.
- 13 Chen, S., P. Liu, L. Chen, and Q. Liu (2020), Evidence from seismological  
14 observation for detecting dynamic change in crustal stress by bedrock temperature  
15 [in Chinese], *Chinese Science Bulletin*, 65(22), 2395-2405, doi:10.1360/TB-  
16 2020-0089.
- 17 Coyner, K. B. (1984), Effects of stress, pore pressure, and pore fluids on bulk strain,  
18 velocity, and permeability of rocks, Ph.D. thesis, Massachusetts Institute of  
19 Technology, Cambridge.
- 20 De Simone, S., V. Vilarrasa, J. Carrera, A. Alcolea, and P. Meier (2013), Thermal  
21 coupling may control mechanical stability of geothermal reservoirs during cold  
22 water injection, *Physics and Chemistry of the Earth, Parts A/B/C*, 64, 117-126,  
23 doi:10.1016/j.pce.2013.01.001.
- 24 Demange, M. (2012), *Mineralogy for petrologists : optics, chemistry, and occurrence*  
25 *of rock-forming minerals*, edited, CRC Press, London,  
26 doi:10.1201/9780429355172.
- 27 Domenico, P. A., and F. W. Schwartz (1998), *Physical and chemical hydrogeology*,  
28 2nd ed., John Wiley, New York.
- 29 Dong, H. (2008), *Micro-CT imaging and pore network extraction*, Ph.D. thesis,  
30 Imperial College London.
- 31 Detournay, E., and A. H. D. Cheng (1993), Fundamentals of Poroelasticity, in  
32 *Comprehensive Rock Engineering: Principles, Practice and Projects*, edited by J.  
33 A. Hudson, pp. 113-171, Pergamon Press, Oxford, UK,  
34 doi:<https://doi.org/10.1016/B978-0-08-040615-2.50011-3>.
- 35 Duhamel JMC (1837), Second mémoire sur les phénomènes thermo-mécaniques  
36 Second memoir on thermo-mechanical phenomena, *Journal de l'Ecole*  
37 *Polytechnique*, Tome 15, Cahier 25, pp 1–57.
- 38 Fulton, P. M., et al. (2013), Low Co-seismic Friction on the Tohoku-Oki Fault  
39 Determined from Temperature Measurements, *Science*, 342(6163), 1214-1217,  
40 doi:10.1126/science.1243641.

- Geertsma J. (1957a), The effect of fluid Pressure decline on volumetric Changes of porous rocks, *Petroleum Transactions, AIME*, 210, 331-340.
- Geertsma, J. (1957b), A remark on the analogy between thermoelasticity and the elasticity of saturated porous media, *Journal of the Mechanics and Physics of Solids*, 6(1), 13-16, doi: 10.1016/0022-5096(57)90042-X.
- Ghassemi, A., and Q. Tao (2016), Thermo-poroelastic effects on reservoir seismicity and permeability change, *Geothermics*, 63, 210-224, doi: 10.1016/j.geothermics.2016.02.006.
- Goodman, R. E. (1989), *Introduction to Rock Mechanics*, 2nd ed., JohnWiley & Sons, New York.
- Green, D. H., and H. F. Wang (1986), Fluid pressure response to undrained compression in saturated sedimentary rock, *Geophysics*, 51(4), 948-956.
- Gurevich, B. (2004), A simple derivation of the effective stress coefficient for seismic velocities in porous rocks, *GEOPHYSICS*, 69(2), 393-397, doi:10.1190/1.1707058.
- Guéguen, Y., and M. Boutéca (2004), *Mechanics of Fluid-Saturated Rocks*, Academic Press.
- Hart, D. J., and H. F. Wang (1995), Laboratory measurements of a complete set of poroelastic moduli for Berea sandstone and Indiana limestone, *Journal of Geophysical Research: Solid Earth*, 100(B9), 17741-17751, doi:10.1029/95JB01242.
- Hashimoto, Y., K. Ujiie, A. Sakaguchi, and H. Tanaka (2007), Characteristics and implication of clay minerals in the northern and southern parts of the Chelung-pu fault, Taiwan, *Tectonophysics*, 443(3), 233-242.
- Hetnarski, R. B., and M. R. Eslami (2008), *Thermal Stresses—Advanced Theory and Applications (Solid Mechanics and Its Applications)*, Springer, Netherlands, doi:https://doi.org/10.1007/978-3-030-10436-8.
- Inazu, D., Y. Ito, D. Saffer, and R. Hino (2014), An abrupt seafloor water-temperature increase in the epicentral region of the 2011 Tohoku earthquake, *Japan Geoscience Union Meeting 2014*.
- Jaeger, J., N. G. Cook, and R. Zimmerman (2007), *Fundamentals of Rock Mechanics*, Blackwell.
- Kano, Y., J. Mori, R. Fujio, H. Ito, T. Yanagidani, S. Nakao, and K.-F. Ma (2006), Heat signature on the Chelungpu fault associated with the 1999 Chi-Chi, Taiwan earthquake, *Geophysical research letters*, 33(14), L14306.
- Lessen, M. (1956), Thermoelasticity and thermal shock, *Journal of the Mechanics and Physics of Solids*, 5(1), 57-61, doi:https://doi.org/10.1016/0022-5096(56)90007-2.
- Li, H., H. Wang, Z. Xu, J. Si, J. Pei, T. Li, Y. Huang, S.-R. Song, L.-W. Kuo, and Z. Sun (2013), Characteristics of the fault-related rocks, fault zones and the principal

- 1 slip zone in the Wenchuan Earthquake Fault Scientific Drilling Project Hole-1
- 2 (WFSD-1), *Tectonophysics*, 584, 23-42.
- 3 Li, H., et al. (2015), Long-term temperature records following the Mw 7.9 Wenchuan
- 4 (China) earthquake are consistent with low friction, *Geology*, 43(2), 163-166,
- 5 doi:10.1130/g35515.1.
- 6 Lide, D. R. (2010), *CRC handbook of chemistry and physics*, 90th Edition (CD-
- 7 ROM Version 2010), CRC press/Taylor and Francis, Boca Raton, Fla.
- 8 Ma, J., L. Liu, P. Liu, and S. Ma (2007), Thermal Precursory Pattern of Fault
- 9 Unstable Slip: An Experimental Study of En Echelon Faults, *Chinese Journal of*
- 10 *Geophysics*, 50(4), 995-1004.
- 11 Ma, J., and X. Shan (2000), An attempt to study fault activity using remote sensing
- 12 technology-A case of the Mani earthquake, *SEISMOLOGY AND GEOLOGY*, 3,
- 13 000.
- 14 Ma, J., S. I. Sherman, and Y. Guo (2012), Identification of meta-instable stress state
- 15 based on experimental study of evolution of the temperature field during stick-
- 16 slip instability on a 5° bending fault, *SCIENCE CHINA Earth Sciences*, 55(6),
- 17 869-881, doi:10.1007/s11430-012-4423-2.
- 18 McTigue, D. F. (1986), Thermoelastic response of fluid-saturated porous rock,
- 19 *Journal of Geophysical Research: Solid Earth* (1978–2012), 91(B9), 9533-9542.
- 20 McTigue, D. F. (1990), Flow to a heated borehole in porous, thermoelastic rock:
- 21 Analysis, *Water Resources Research*, 26(8), 1763-1774,
- 22 doi:10.1029/WR026i008p01763.
- 23 Meng, F., X. Li, P. Baud, and T. f. Wong (2020), Effective Stress Law for the
- 24 Permeability and Pore Volume Change of Clayey Sandstones, *Journal of*
- 25 *Geophysical Research: Solid Earth*, 125(8), doi:10.1029/2020jb019765.
- 26 Milne, J. (1913), *Earthquakes and other earth movements*, London.
- 27 Mosenfelder, J. L., P. D. Asimow, and T. J. Ahrens (2007), Thermodynamic
- 28 properties of Mg<sub>2</sub>SiO<sub>4</sub> liquid at ultra-high pressures from shock measurements to
- 29 200 GPa on forsterite and wadsleyite, *Journal of Geophysical Research: Solid*
- 30 *Earth*, 112(B6), B06208, doi:10.1029/2006JB004364.
- 31 Müller, T., and P. Sahay (2016), Biot coefficient is distinct from effective pressure
- 32 coefficient, *GEOPHYSICS*, 81, L1-L7, doi:10.1190/geo2015-0625.1.
- 33 Müller, T. M., and P. N. Sahay (2019), Elastic potential energy in linear
- 34 poroelasticity, *Geophysics*, 84(4), W1-W20, doi:10.1190/geo2018-0216.1.
- 35 Neumann F (1885), *Vorlesung über die Theorie des Elasticität der festen Körper*
- 36 *und des Lichtäthers*. Teubner, Leipzig (Meyer, Breslau).
- 37 Neuzil, C. E. (2003), Hydromechanical coupling in geologic processes,
- 38 *Hydrogeology Journal*, 11(1), 41-83.
- 39 Njiekak, G., and D. R. Schmitt (2019), Effective Stress Coefficient for Seismic
- 40 Velocities in Carbonate Rocks: Effects of Pore Characteristics and Fluid Types,



- Pure and Applied Geophysics*, 176(4), 1467-1485, doi:10.1007/s00024-018-2045-0.
- Norris, A. (1992), On the correspondence between poroelasticity and thermoelasticity, *Journal of Applied Physics*, 71(3), 1138-1141, doi:10.1063/1.351278.
- Nowacki, W. (1986), *Thermoelasticity*, 2nd ed., PWN-Polish Scientific Publishers, Warsaw, and Pergamon Press, Oxford, doi:10.1016/C2013-0-03247-1.
- Nur, A., and J. D. Byerlee (1971), An exact effective stress law for elastic deformation of rock with fluids, *Journal of Geophysical Research*, 76(26), 6414-6419, doi:10.1029/JB076i026p06414.
- Orihara, Y., M. Kamogawa, and T. Nagao (2014), Preseismic Changes of the Level and Temperature of Confined Groundwater related to the 2011 Tohoku Earthquake, *Scientific reports*, 4, doi:10.1038/srep06907.
- Ouzounov, D., and F. Freund (2004), Mid-infrared emission prior to strong earthquakes analyzed by remote sensing data, *Advances in Space Research*, 33(3), 268-273.
- Palciauskas, V. V., and P. A. Domenico (1989), Fluid pressures in deforming porous rocks, *Water Resources Research*, 25(2), 203-213, doi:10.1029/WR025i002p00203.
- Pan, Z. (1993), *Crystallography and mineralogy*, 3rd Edition [in Chinese], Geological Publishing House, Beijing.
- Paterson, M. S., and T.-f. Wong (2005), *Experimental Rock Deformation — The Brittle Field*, 2nd ed., Springer-Verlag, Berlin.
- Qin, Y., X. Yang, B. Wu, Z. Sun, and X. Shi (2013), High resolution temperature measurement technique for measuring marine heat flow, *Sci. China Technol. Sci.*, 56(7), 1773-1778, doi:10.1007/s11431-013-5239-9.
- Rice, J. R., and M. P. Cleary (1976), Some basic stress diffusion solutions for fluid-saturated elastic porous media with compressible constituents, *Rev. Geophys. Space Phys*, 14(2), 227-241, doi:10.1029/RG014i002p00227.
- Richter, D., and G. Simmons (1974), Thermal expansion behavior of igneous rocks, paper presented at International Journal of Rock Mechanics and Mining Sciences & Geomechanics Abstracts, Elsevier.
- Sahay, P. N. (2013), Biot constitutive relation and porosity perturbation equation, *GEOPHYSICS*, 78(5), L57-L67, doi:10.1190/geo2012-0239.1.
- Salimzadeh, S., A. Paluszny, H. M. Nick, and R. W. Zimmerman (2018), A three-dimensional coupled thermo-hydro-mechanical model for deformable fractured geothermal systems, *Geothermics*, 71, 212-224, doi:10.1016/j.geothermics.2017.09.012.
- Schön, J. H. (2011), *Physical properties of rocks: a workbook*, Elsevier, Oxford.
- Skempton, A. (1954), The pore-pressure coefficients A and B, *Géotechnique*, 4(4),

- 143-147.
- Stixrude, L., and C. Lithgow-Bertelloni (2005), Thermodynamics of mantle minerals – I. Physical properties, *Geophysical Journal International*, 162(2), 610-632, doi:10.1111/j.1365-246X.2005.02642.x.
- Tanaka, H., W. Chen, K. Kawabata, and N. Urata (2007), Thermal properties across the Chelungpu fault zone and evaluations of positive thermal anomaly on the slip zones: Are these residuals of heat from faulting?, *Geophysical research letters*, 34(1).
- Tanaka, H., W. Chen, C. Wang, K. Ma, N. Urata, J. Mori, and M. Ando (2006), Frictional heat from faulting of the 1999 Chi - Chi, Taiwan earthquake, *Geophysical research letters*, 33(16).
- Teng, T., Y. Zhao, F. Gao, J. G. Wang, and W. Wang (2018), A fully coupled thermo-hydro-mechanical model for heat and gas transfer in thermal stimulation enhanced coal seam gas recovery, *International Journal of Heat and Mass Transfer*, 125, 866-875, doi:10.1016/j.ijheatmasstransfer.2018.04.112.
- Terzaghi, K. (1923), Die Berechnung der Durchlässigkeitziffer des Tones aus dem Verlauf der hydrodynamischen Spannungserscheinungen [The computation of permeability of clays from the progress of hydrodynamic strain]. *Akad der Wissenschaften in Wien, Sitzungsberichte, Mathematisch-naturwissenschaftliche Klasse, Part Ila*, 132(3/4), pp 125–138
- Tronin, A. A., M. Hayakawa, and O. A. Molchanov (2002), Thermal IR satellite data application for earthquake research in Japan and China, *Journal of Geodynamics*, 33(4), 519-534.
- Turcotte, D., and G. Schubert (2014), *Geodynamics*, 3rd ed., Cambridge University Press, Cambridge, U. K.
- Waldbaum, D. R. (1971), Temperature Changes associated with Adiabatic Decompression in Geological Processes, *Nature*, 232(5312), 545-547.
- Wang, C., M. Manga, C. Wang, and C. Chin (2012), Transient change in groundwater temperature after earthquakes, *Geology*, 40, 119-122.
- Wang, C. Y., L. P. Wang, M. Manga, C. H. Wang, and C. H. Chen (2013), Basin - scale transport of heat and fluid induced by earthquakes, *Geophysical Research Letters*, 40(15), 3893-3897.
- Wang, H. F. (2000), *Theory of linear poroelasticity with applications to geomechanics and hydrogeology*, edited, Princeton University Press, New Jersey.
- Wang, H. F., B. P. Bonner, S. R. Carlson, B. J. Kowalls, and H. C. Heard (1989), Thermal stress cracking in granite, *Journal of Geophysical Research*, 94(B2), 1745-1758.
- Wang, H., H. Li, J. Si, Z. Sun, and Y. Huang (2014), Internal structure of the Wenchuan earthquake fault zone, revealed by surface outcrop and WFSD-1

- drilling core investigation, *Tectonophysics*, 619–620, 101-114, doi:10.1016/j.tecto.2013.08.029.
- Wang, L., and C. Zhu (1984), Anomalous variations of ground temperature before the Tangsan and Haiheng earthquakes, *J. Seismol. Res*, 7(6), 649-656.
- Wong, A. K., R. Jones, and J. G. Sparrow (1987), Thermoelastic constant or thermoelastic parameter?, *Journal of Physics and chemistry of solids*, 48(8), 749-753.
- Wong, A. K., J. G. Sparrow, and S. A. Dunn (1988), On the revised theory of the thermoelastic effect, *Journal of Physics and chemistry of solids*, 49(4), 395-400, doi:http://dx.doi.org/10.1016/0022-3697(88)90099-6.
- Wong, T.-f., and W. Brace (1979), Thermal expansion of rocks: some measurements at high pressure, *Tectonophysics*, 57(2), 95-117.
- Xiao, Y., R. Zheng, and J. Deng (2017), *Petrology introduction*, 4th Edition [in Chinese], Geological Publishing House, Beijing.
- Yang, S. M., and W. Q. Tao (2006), *Heat transfer*, 4th Edition [in Chinese], Higher Education Press, Beijing.
- Yang, X., W. Lin, O. Tadai, X. Zeng, C. Yu, E.-C. Yeh, H. Li, and H. Wang (2017), Experimental and numerical investigation of the temperature response to stress changes of rocks, *Journal of Geophysical Research: Solid Earth*, 122(7), 5101-5117, doi:10.1002/2016JB013645.
- Yang, X., W. Lin, O. Tadai, X. Zeng, X. Shi, and Z. Xu (2018), System for determining the adiabatic stress derivative of temperature for rock. US2018/0038812 A1.
- Yang, X., W. Lin, E.-C. Yeh, H. Xu, and Z. Xu (2020), Analysis on the mechanisms of co-seismic temperature negative anomaly in fault zones [in Chinese], *Chinese Journal of Geophysics*, 63(4), 1422-1430, doi:10.6038/cjg2020M0638.
- Yang, X., W. Lin, O. Tadai, H. Xu, X. Zeng (2020), Temperature response of water-saturated compact Longmenshan limestone and porous Rajasthan sandstone to changes in confining pressure [Data set]. *Zenodo*. <http://doi.org/10.5281/zenodo.4242969>.
- Zimmerman, R. W. (2000), Coupling in poroelasticity and thermoelasticity, *International Journal of Rock Mechanics and Mining Sciences*, 37(1), 79-87, doi: 10.1016/S1365-1609(99)00094-5.

# **Figure captions and Tables:**

**Figure 1.** (a) Correlation between effective stress coefficient ( $a$ ) and porosity ( $\phi$ ) where FL01 (the black line) is the linear fitting result for all 15 rocks, the pink dash line is  $a = \phi$ . The red and blue lines represent the maximum and minimum, respectively (similarly hereinafter). (b) Correlation

between poroelastic expansion coefficient  $1/H$  and  $\phi$  for all 15 rock samples where FL02 (the black line) is the linear fitting result. (c) The trend of Skempton's coefficient  $B$  with  $\phi$ .

**Figure 2.** Graphical illustration of the calculated values of  $\beta_{\text{wet}_U}$  for 15 rock samples under undrained conditions. For each rock sample, the Skempton's coefficient  $B$  is in the 0–1 range; and the range of effective stress coefficient  $a$  is estimated from porosity  $\phi$  based on Equation (28).

**Figure 3.** Apparatus setup for quasi-undrained conditions. (a) Diagrammatic sketch of rock specimen assembly. (b) The local structure around temperature sensor T01 (shown in green). (c, d, and e) Photographs of rock specimen assembly before and after being enveloped with rubber jacket and O-rings. HS, SS, RJ, HR, ST and TG are hard silicone (pink), soft silicone (dark gray), rubber jacket (orange), hard rubber (black), steel tube (light gray), and thermally conductive silicone grease (yellow), respectively. There is filled with water in the gap between rock specimen and steel tube. The temperature sensor size is  $1.95 \text{ mm} \times 1.25 \text{ mm} \times 0.93 \text{ mm}$ . The wire diameter is 0.2 mm.

**Figure 4.** Apparatus setup for quasi-drained conditions. (a) Diagrammatic sketch of rock specimen assembly. (b) The local structure around temperature sensor T01 (shown in green).

**Figure 5.** Changes in confining pressure in Vessel B ( $\Delta P$ ) and temperature ( $\Delta T$ ) during the unloading/loading processes of water-saturated Rajasthan sandstone (RJS(W)) under quasi-undrained conditions. T01 is in the rock specimen center, T02 is on the sample surface, and T03 is in oil in Vessel B. For each test, the background temperature  $T_0$  ( $\sim 22.5\text{--}24.0^\circ\text{C}$ , Table 3) was removed, only temperature change was shown here. In these testes, the initial times represent the moments of rapid loading/unloading (similarly hereinafter).

**Figure 6.** Changes in confining pressure in Vessel B ( $\Delta P$ ) and temperature ( $\Delta T$ ) during the unloading/loading processes of water-saturated Rajasthan sandstone (RJS(W)) under quasi-drained conditions.

**Figure 7.** Changes in confining pressure in Vessel B ( $\Delta P$ ) and temperature ( $\Delta T$ ) during the loading/unloading processes of water-saturated Longmensan limestone (L27(W)) under quasi-drained conditions.

**Figure 8.** Calculated lower and upper limits of  $\beta_{\text{wet}}$  for all 15 rock samples when (a) Porosity ( $\phi$ ) is within 0.05 and (b) porosity ( $\phi$ ) ranges from 0.05 to 0.30. Red and pink circles represent the upper limits under undrained ( $\beta_{\text{wet}_U\_Max}$ ) and drained ( $\beta_{\text{wet}_D\_Max}$ ) conditions, respectively. Blue and green circles represent the lower limits in both undrained ( $\beta_{\text{wet}_U\_Min}$ ) and drained ( $\beta_{\text{wet}_D\_Min}$ ) conditions, respectively. Pink dots represent  $\beta_{\text{wet}_U}$  when  $B$  is 0.5 ( $\beta_{\text{wet}_U(B=0.5)}$ ). Blue triangles represent the lower limit under undrained conditions with Skempton's coefficient  $B = 0.5$ . Black circles represent the measured  $\beta$  of dry rocks ( $\beta_{\text{dry}}$ ) [Yang *et al.*, 2017]. Orange stars denote measured values of  $\beta_{\text{wet}}$  in tests RJS(W)-13 to -18 and L27(W)-01 to -03.

**Table 1.** Collected laboratory data on poroelastic constants for compact and porous rocks [Berryman, 1992; Wang, 2000; Paterson and Wong, 2005]

No.	Rock	$\phi$	$K$ (GPa)	$K_s$ (GPa)	$B$	$\alpha$	$1/H$ (GPa <sup>-1</sup> )	Pressure (MPa)	Reference
1	Barre	0.027	15.0	53.0	0.62	0.72	0.04780	$P_c - P_f \sim 10$	[Mesri et al., 1976]
2	Charcoal	0.020	35.0	45.0	0.55	0.22	0.00635		[Rice and Cleary, 1976]
3	Granite	0.010	25.0	45.0	0.85	0.44	0.01778		[Rice and Cleary, 1976]
4	Westerly	0.008	24.0	53.0		0.55	0.02280	$P_c = 10$	[Coyner, 1984; Berryman, 1992]
5	Westerly (red)	0.008	34.0	54.0		0.37	0.01089	$P_c = 25$	[Coyner, 1984; Berryman, 1992]
6	Chelmsford	0.011	17.0	55.5		0.69	0.04081	$P_c = 25$	[Coyner, 1984; Berryman, 1992]
7	Tennessee marble	0.020	40.0	50.0	0.51	0.20	0.00500		[Rice and Cleary, 1976]
8	Vermont marble	0.021	25.0	69.0	0.46	0.64	0.02551	$P_c - P_f \sim 10$	[Mesri et al., 1976]
9	Salem limestone	0.126	13.0	38.0	0.32	0.66	0.05061	$P_c - P_f \sim 10$	[Mesri et al., 1976]
10	Indiana limestone	0.130	21.2	72.6	0.46	0.71	0.03340	$P_c - \alpha \cdot P_f \sim 20-35$	[Hart and Wang, 1995]
11	Carbonate	0.130	19.3	41.4	0.20	0.53	0.02766		[Fabre and Gustkiewicz, 1997]
12	Tonnerre limestone	0.165	16.3	52.6	0.20	0.69	0.04234	$P_c \sim 100$	[Fabre and Gustkiewicz, 1997]
13	Chauvigny limestone	0.219	13.8	58.9	0.30	0.77	0.05549	$P_c \sim 50$	[Fabre and Gustkiewicz, 1997]
14	Lavoux limestone	0.428	3.8	42.5	0.35	0.91	0.23963		[Fabre and Gustkiewicz, 1997]
15	Lixhe chalk	0.119	23.0	66.0		0.65	0.02833	$P_c = 10$	[Coyner, 1984; Berryman, 1992]
16	Bedford limestone	0.119	27.0	66.0		0.59	0.02189	$P_c = 25$	[Coyner, 1984; Berryman, 1992]
17	Boise	0.260	4.6	42.0	0.50	0.89	0.19358		[Detournay and Cheng, 1993]
18	Ohio	0.190	8.4	31.0	0.50	0.73	0.08679		[Detournay and Cheng, 1993]
19	Pecos	0.200	6.7	39.0	0.61	0.83	0.12361		[Detournay and Cheng, 1993]
20	Fontainebleau	0.060	30.9	35.2	0.25	0.12	0.00395	$P_c = 90$	[Fabre and Gustkiewicz, 1997]
21	Sandstone	0.170	17.4	42.5	0.46	0.59	0.03394		[Fabre and Gustkiewicz, 1997]
22	Vosges (yellow)	0.180	13.9	38.6	0.35	0.64	0.04604		[Fabre and Gustkiewicz, 1997]
23	Vosges (red)	0.190	8.0	36.0	0.62	0.78	0.09722		[Rice and Cleary, 1976]
24	Berea	0.190	6.6	28.9	0.75	0.77	0.11691	$P_c - \alpha \cdot P_f = 10$	[Hart and Wang, 1995]
25	Berea	0.203	4.7	36.3	0.53	0.87	0.18522	$P_c - P_f \sim 10$	[Mesri et al., 1976]

26	Berea	0.178	6.0	39.0	0.85	0.14103	Pc = 10	[Coyner, 1984; Berryman, 1992]
27	Berea	0.178	10.0	39.0	0.74	0.07436	Pc = 25	[Coyner, 1984; Berryman, 1992]
28	Navajo	0.118	13.0	34.0	0.62	0.04751	Pc = 10	[Coyner, 1984; Berryman, 1992]
29	Navajo	0.118	16.5	34.5	0.52	0.03162	Pc = 25	[Coyner, 1984; Berryman, 1992]
30	Weber	0.095	10.0	38.0	0.74	0.07368	Pc = 25	[Coyner, 1984; Berryman, 1992]
31	Weber	0.060	13.0	36.0	0.73	0.64	0.04915	[Rice and Cleary, 1976]
32	Ruhr	0.020	13.0	36.0	0.88	0.64	0.04915	[Rice and Cleary, 1976]

Note:  $\phi$ ,  $K$  and  $K_s$  are porosity, bulk modulus of dry aggregate and intrinsic bulk modulus of solid grains, respectively.  $B$ ,  $a$  and  $1/H$  are Skempton's coefficient, effective stress coefficient and poroelastic expansion coefficient, respectively.

**Table 2.** Physical Properties of the all 15 Rock Samples\* and the estimated ranges of  $\beta_{\text{wet\_U}}$  and  $\beta_{\text{wet\_D}}$

No.	Sample ID	Lithology or Material	$\phi$	$(\rho c)_{\text{dry}}$ (MJ/(m <sup>3</sup> . K))	$\beta_{\text{dry}}$ (mK/MPa)	Range of $\alpha$	Range of $\beta_{\text{wet\_U}}$ when $B = 0-1$ (mK/MPa)	Range of $\beta_{\text{wet\_U}}$ when $B = 0.5-1.0$ (mK/MPa)	Range of $1/H$ (GPa <sup>-1</sup> )	Range of $\beta_{\text{wet\_D}}$ when $ \Delta P_c  \leq 15$ MPa (mK/MPa)	Note
1	L27	Limestone	0.003	2.287	1.53	0.403-0.703	0.54-1.52	1.03-1.52	0.000-0.063	1.52-1.55	From LMS Fault Zone
2	L35	Granite	0.005	2.352	3.16	0.406-0.706	1.08-3.13	2.10-3.13	0.000-0.064	3.13-3.18	From LMS Fault Zone
3	L24	Granodiorite	0.006	2.026	2.92	0.407-0.707	1.07-2.88	1.97-2.88	0.000-0.065	2.88-2.94	From LMS Fault Zone
4	L31	Lithic sandstone	0.012	2.158	3.58	0.412-0.712	1.39-3.50	2.45-3.50	0.000-0.067	3.50-3.57	From LMS Fault Zone
5	L25	Cataclasite	0.012	2.245	4.24	0.413-0.713	1.58-4.15	2.87-4.15	0.000-0.068	4.15-4.23	From LMS Fault Zone
6	L20	Sandstone	0.017	1.614	4.10	0.417-0.717	1.84-3.93	2.89-3.93	0.000-0.070	3.93-4.04	From LMS Fault Zone, black fault breccia
7	L23	Sandstone	0.019	1.869	4.35	0.420-0.720	1.90-4.18	3.04-4.18	0.000-0.071	4.17-4.27	From LMS Fault Zone, black fault breccia
8	L17	Sandstone	0.043	1.750	4.03	0.443-0.743	2.58-3.68	3.12-3.68	0.000-0.083	3.65-3.75	From LMS Fault Zone, black fault breccia
9	KBT	Basalt	0.076	1.967	2.69	0.475-0.775	2.32-3.66	2.64-3.66	0.000-0.099	2.32-2.38	From Karatsu, Saga Prefecture, Japan
10	L28	Siltstone	0.100	1.261	3.66	0.499-0.799	2.75-5.77	3.85-5.77	0.000-0.111	2.75-2.87	From LMS Fault Zone
11	RJS	Sandstone	0.102	1.737	4.71	0.500-0.800	3.78-5.37	4.01-5.37	0.000-0.112	3.78-3.91	From Rajasthan, India
12	C01	Siltstone	0.110	1.991	4.28	0.509-0.809	3.48-5.03	3.73-5.03	0.000-0.116	3.48-3.59	From TCDP Hole-A, Chelungpu Fault. The depth is 1105.43-1105.73 m
13	C02	Sandstone with bioturbation	0.122	2.192	4.81	0.520-0.820	3.90-5.21	3.97-5.21	0.002-0.122	3.90-4.02	From TCDP Hole-A, Chelungpu Fault. The depth is 484.75~484.93 m
14	BRS	Sandstone	0.200	1.528	5.86	0.579-0.879	3.79-7.78	5.21-7.78	0.041-0.161	3.79-3.96	From Berea, Ohio, USA
15	TTF	Welded tuff	0.300	1.471	6.15	0.694-0.994	3.32-9.14	5.73-9.14	0.091-0.211	3.32-3.49	From Toge, Tochigi Prefecture, Japan

\*  $\phi$ ,  $(\rho c)_{\text{dry}}$  and  $\beta_{\text{dry}}$  are the measured porosity, volumetric heat capacity and adiabatic pressure derivative of the temperature  $(\partial T/\partial P)_s$  of the dry rock sample at room temperature [Yang *et al.*, 2017].  
Ranges of  $\alpha$  and  $1/H$  were estimated from porosity  $\phi$  based on equations (28) and (29), respectively. Ranges of  $\beta_{\text{wet\_U}}$  and  $\beta_{\text{wet\_D}}$  are calculated according to equations (19) and (27), respectively.

**Table 3.** Key Experimental Records and Results of Water-Saturated Rock Samples and Tap Water during Loading/Unloading Processes<sup>a</sup>

No.	Sample ID	Test	$T_0$ (°C)	$P_0$ (MPa)	$P_{\text{End}}$ (MPa)	$\Delta P$ (MPa)	$\Delta T$ (mK)	$\beta_{\text{wet\_Meas}}$ (mK/MPa)	Conditions
1	RJS(W)	-13	22.725	3.39	-0.04	-3.43	-22.93	6.68	Quasi-undrained
2	RJS(W)	-14	22.497	6.96	-0.04	-6.99	-42.20	6.04	Quasi-undrained
3	RJS(W)	-15	23.619	-0.07	9.32	9.39	43.30	4.61	Quasi-undrained
4	RJS(W)	-16	23.737	4.79	-0.01	-4.80	-17.15	3.57	Quasi-drained
5	RJS(W)	-17	23.369	9.78	-0.01	-9.79	-35.32	3.61	Quasi-drained
6	RJS(W)	-18	23.356	2.08	15.05	12.97	46.50	3.59	Quasi-drained
7	L27(W)	-01	23.442	0.00	6.83	6.83	10.30	1.50	Quasi-drained
8	L27(W)	-02	23.186	6.90	-0.04	-6.94	-6.38	0.92	Quasi-drained
9	L27(W)	-03	23.893	9.86	-0.03	-9.89	-9.37	0.95	Quasi-drained
10	WT <sup>b</sup>	-01	21.233	50.00	0.00	-50.00	-882.10	17.64	
11	WT <sup>b</sup>	-02	21.231	50.00	0.00	-50.00	-885.30	17.71	
12	WT <sup>c</sup>	-03	31.156	10.03	21.17	11.14	290.00	26.03	

<sup>a</sup>  $T_0$  is the background temperature before loading/unloading.  $P_0$  and  $P_{\text{End}}$  are the initial and end confining pressure in Vessel B during loading/unloading process, respectively.  $\Delta P$  and  $\Delta T$  are the changes in confining pressure in Vessel B and temperature in the center of rock specimen during loading/unloading process, respectively.  $\beta_{\text{wet}}$  is the measurement result of the adiabatic pressure derivative of temperature of water-saturated rock under undrained condition at  $T_0$  for each test.

<sup>b</sup> The results were from two temperature loggers, #002 and #107, in a big pressure vessel filled with tap water during unloading process, at the Guangzhou Marine Geological Survey, China.

<sup>c</sup> The result was from the temperature logger, #095949, in a big pressure vessel filled with tap water during loading process, at the Hadal Science and Technology Research Center, Shanghai Ocean University, China.



**Figure captions:**

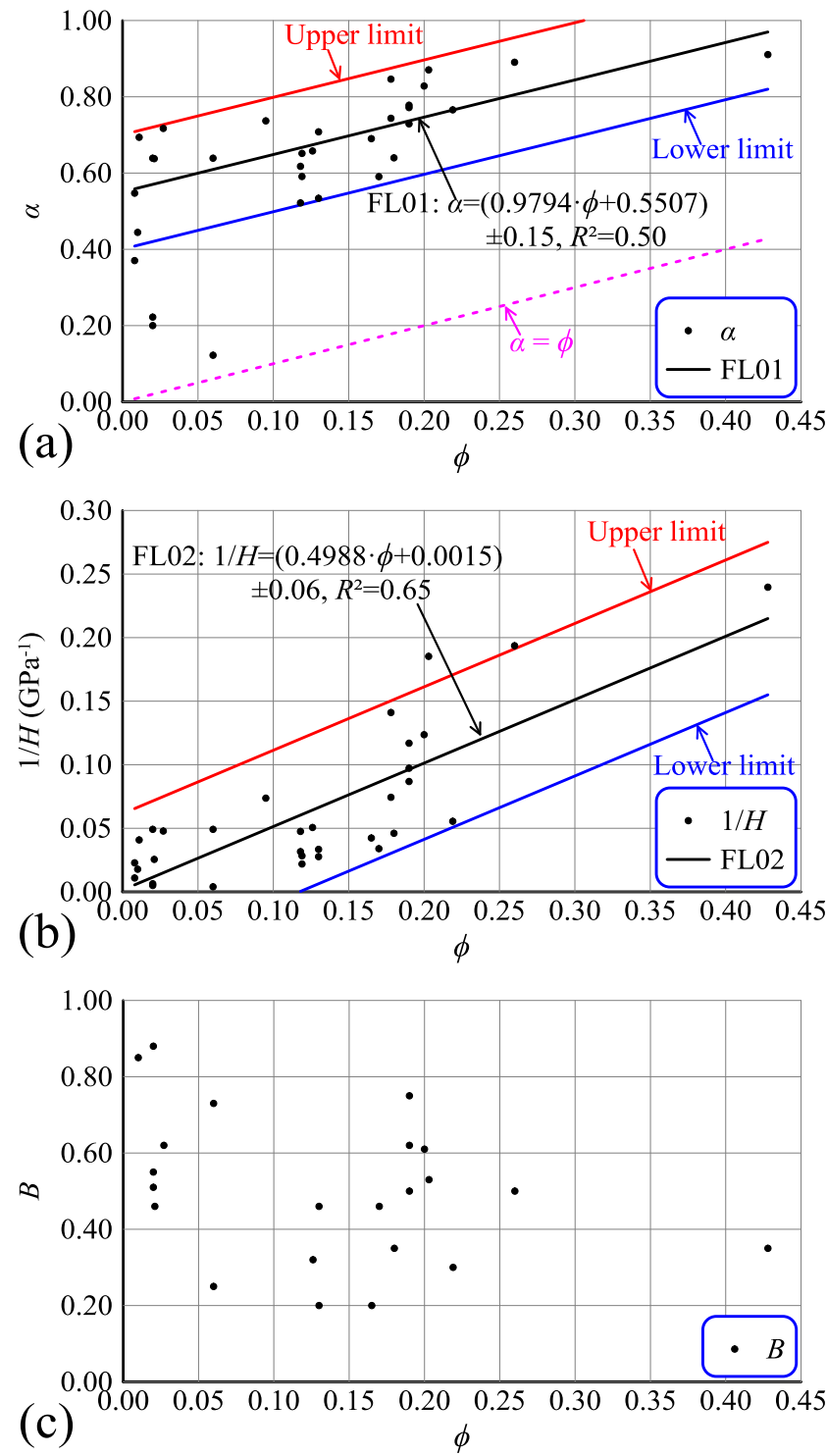


**Figure 1.** (a) Correlation between effective stress coefficient ( $\alpha$ ) and porosity ( $\phi$ ) where the black line (FL01) is the linear fitting curve for all 15 rock samples, the pink dash line is  $\alpha = \phi$ . The red and blue lines represent the upper and lower limits, respectively (similarly hereinafter). (b) Correlation between poroelastic expansion coefficient  $1/H$  and  $\phi$  for all 15 rock samples where the black line (FL02) is the linear fitting curve. (c) The trend of Skempton's coefficient  $B$  with  $\phi$ .

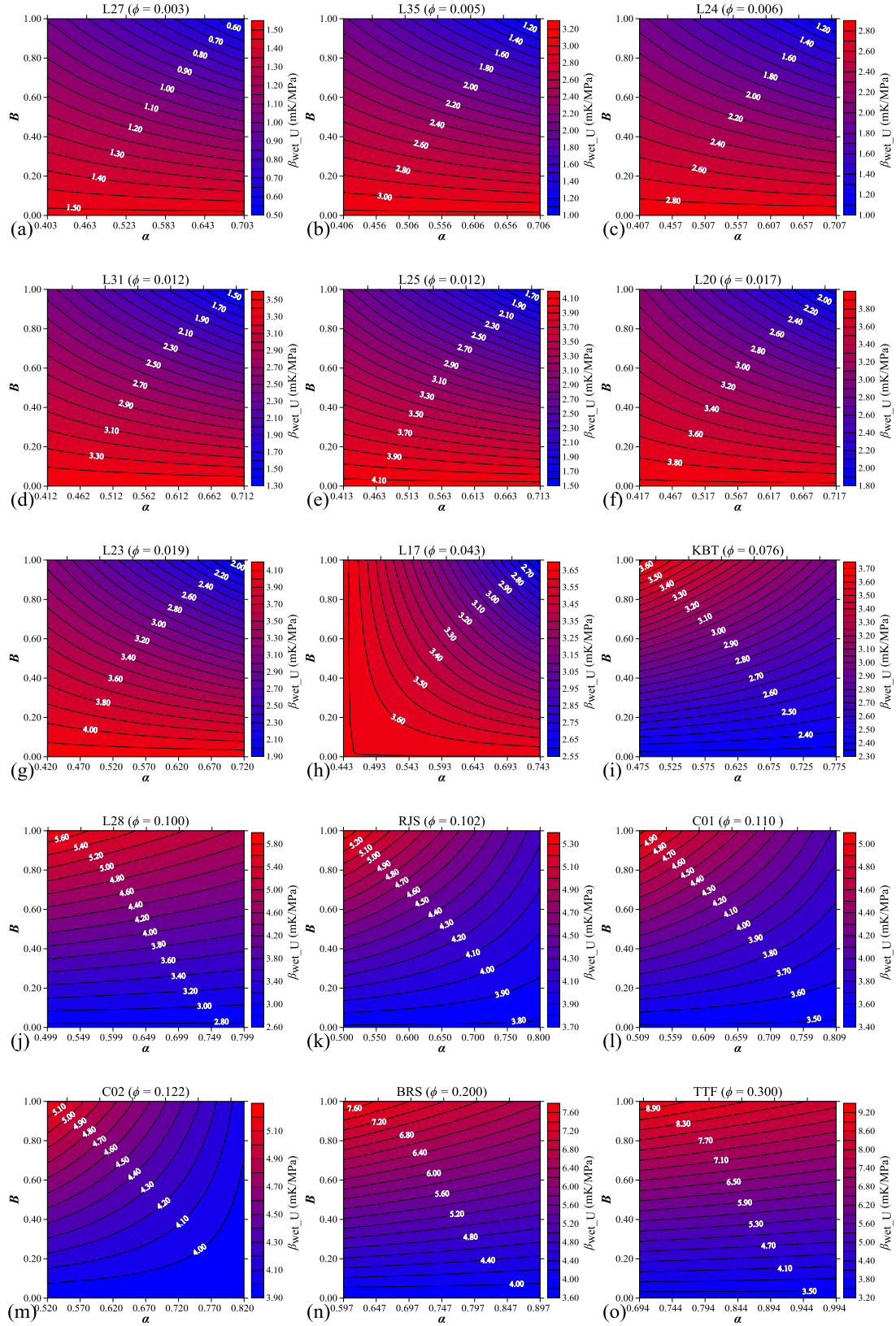


**Figure 2.** Graphical illustration of the calculated values of  $\beta_{\text{wet\_U}}$  for 15 rock samples under undrained conditions. For each rock sample, the Skempton's coefficient  $B$  is in the 0–1 range; and the range of effective stress coefficient  $\alpha$  is estimated from porosity  $\phi$  based on equation (18).

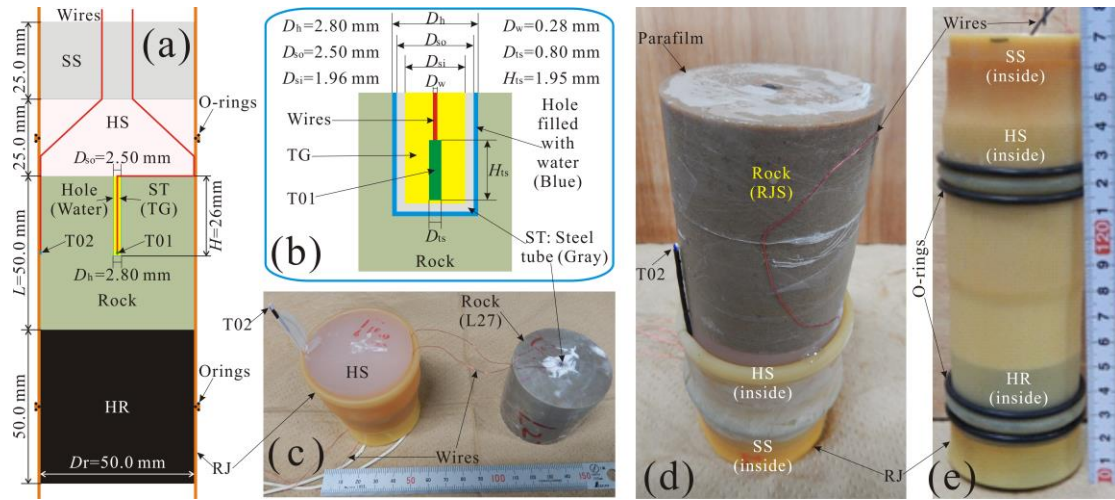


**Figure 3.** Apparatus setup for quasi-undrained conditions. (a) Schematic diagram of rock specimen assembly. (b) Local structure around temperature sensor T01 (shown in green). (c, d) Photographs of rock specimen assembly before being enveloped with rubber jacket and O-rings and (e) after being enveloped with rubber jacket and O-rings. HS is hard silicone (pink), SS is soft silicone (dark gray), RJ is rubber jacket (orange), HR is hard rubber (black), ST is steel tube (light gray) (water is placed in the gap between rock specimen and ST) and TG is thermally conductive silicone grease (yellow). The size of miniature temperature sensors is  $1.95 \text{ mm} \times 1.25 \text{ mm} \times 0.93 \text{ mm}$  and the diameter of the wires is  $0.2 \text{ mm}$ . The equivalent diameters of T01 and the two wires are  $0.8 \text{ mm}$  and  $0.28 \text{ mm}$ , respectively.

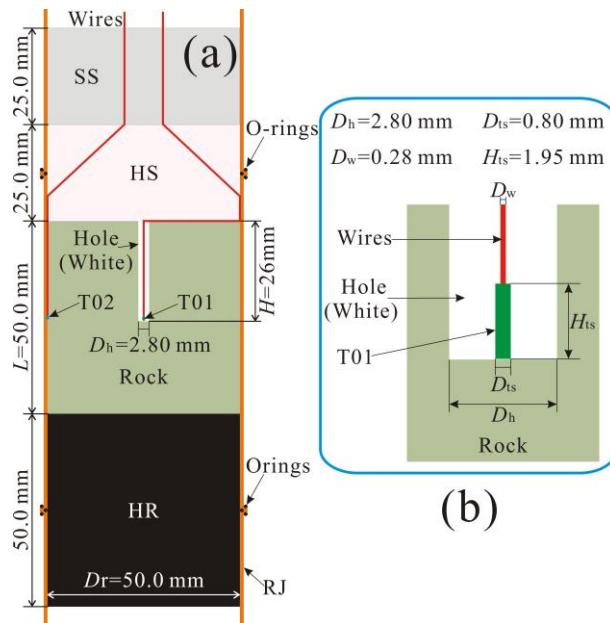


**Figure 4.** Apparatus setup for quasi-drained conditions. (a) Schematic diagram of rock specimen assembly. (b) Local structure around temperature sensor T01 (shown in green).

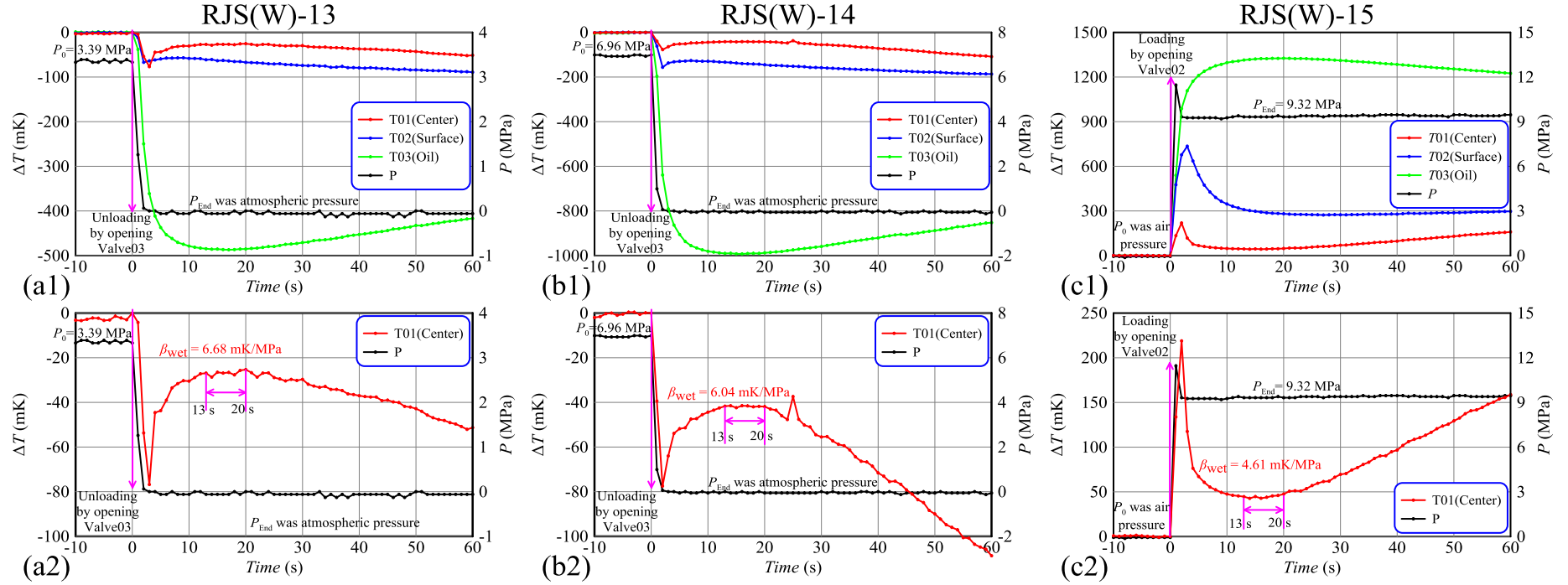


**Figure 5.** Changes of confining pressure ( $\Delta P$ , in Vessel B) and temperature ( $\Delta T$ ) during the unloading/loading processes of water-saturated Rajasthan sandstone (RJS(W)) under quasi-undrained conditions. T01 is in the rock sample center, T02 is on the surface of sample, and T03 is in oil in Vessel B. For each test, the background temperature  $T_0$  ( $\sim 22.5$ – $24.0^\circ\text{C}$ , Table 3) was removed, only temperature change was shown here. In these tests, the points of rapid loading/unloading are set to be the initial times (similarly hereinafter).

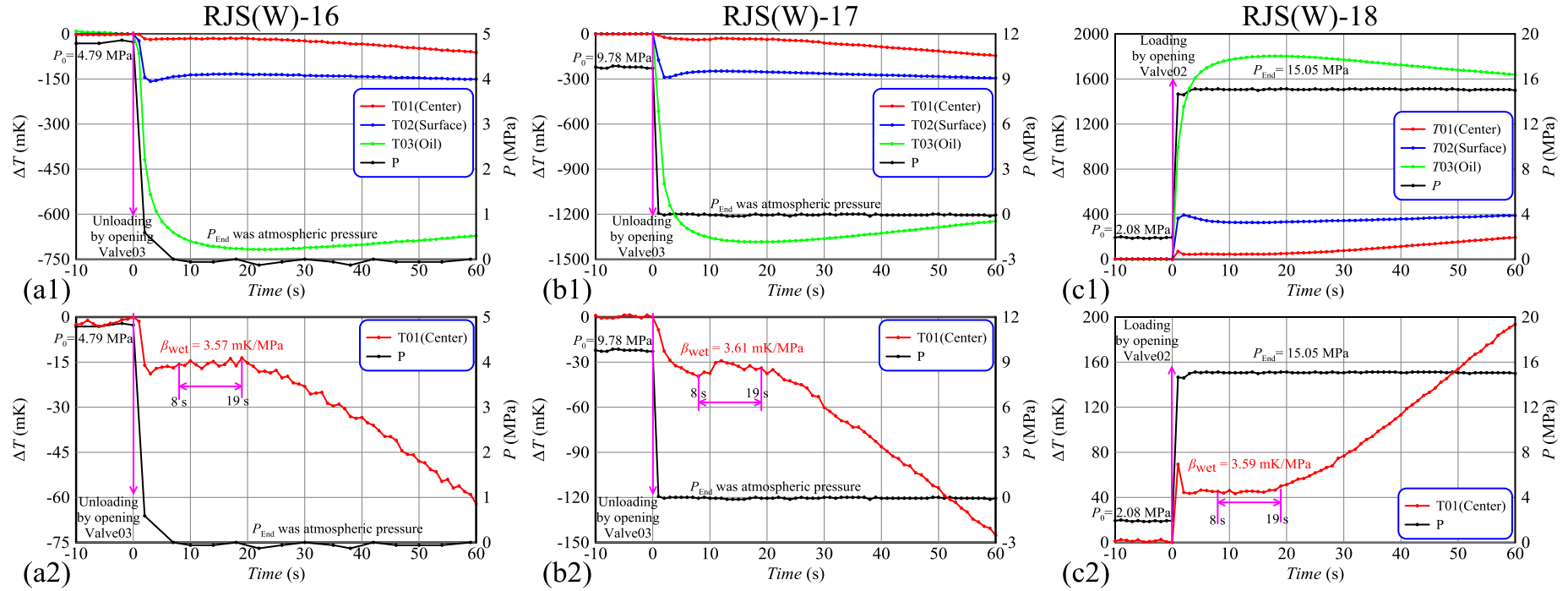


**Figure 6.** Changes of confining pressure ( $\Delta P$ , in Vessel B) and temperature ( $\Delta T$ ) during the unloading/loading processes of water-saturated Rajasthan sandstone (RJS(W)) under quasi-drained conditions.

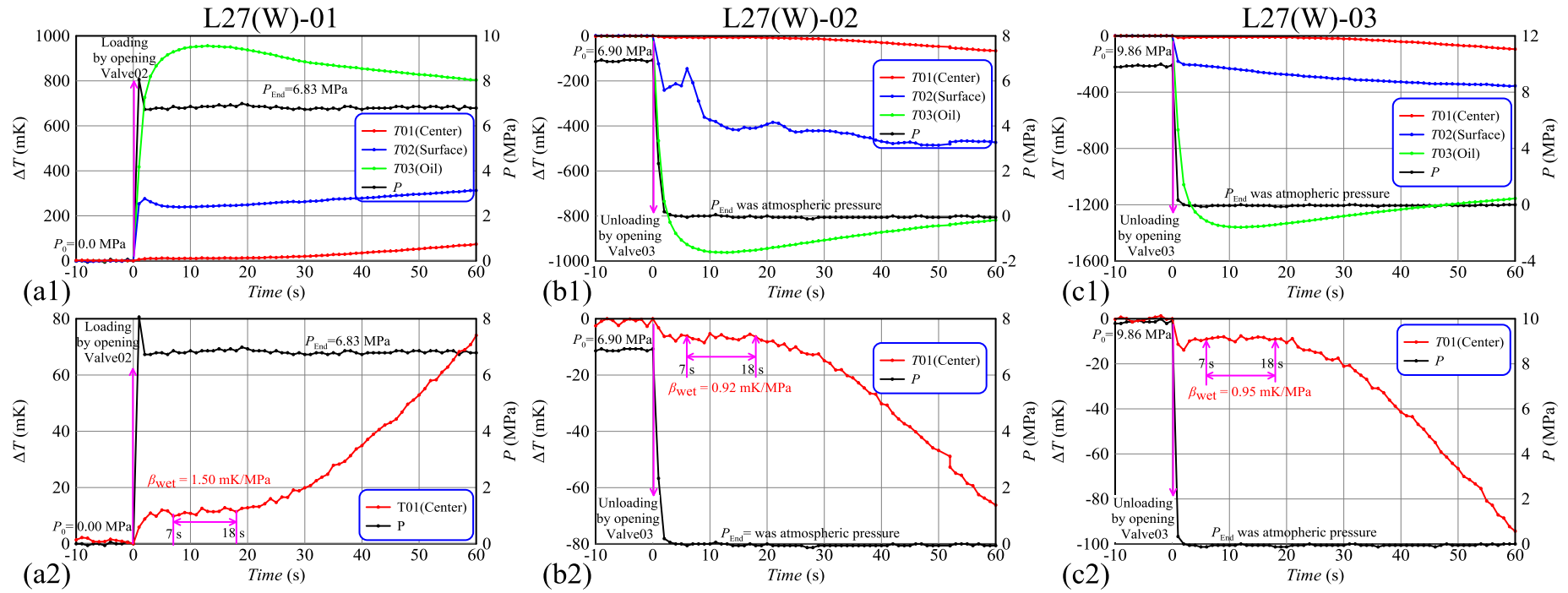


**Figure 7.** Changes of confining pressure ( $\Delta P$ , in Vessel B) and temperature ( $\Delta T$ ) during the loading/unloading processes of water-saturated Longmenshan limestone (L27(W)) under quasi-drained conditions.



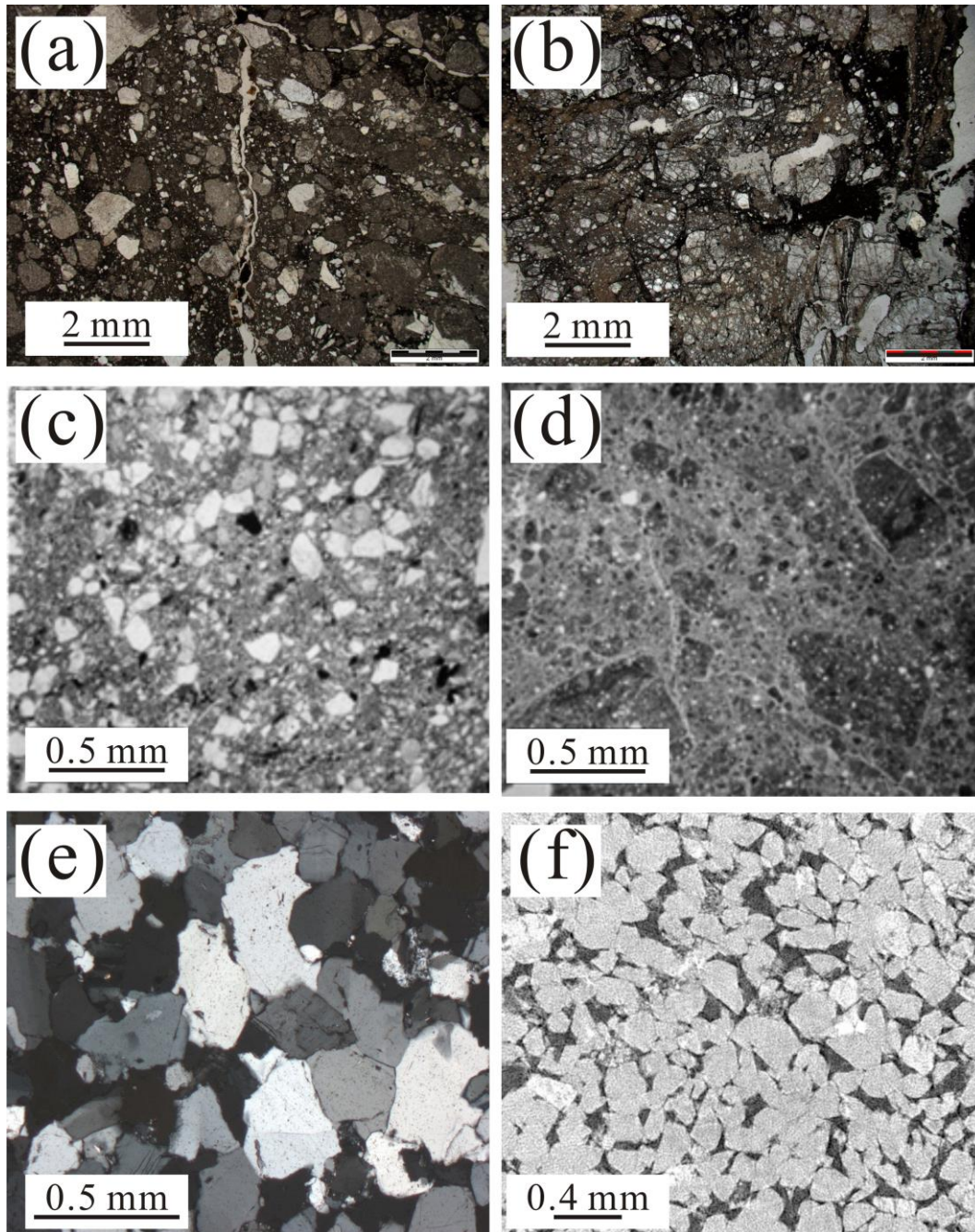


**Figure 8.** (a-b) Photomicrographs of thin sections (in polarized light) of cataclasite and fault breccia from the Longmenshan Fault Zone [Wang *et al.*, 2014]. (c-d) Photomicrographs of thin sections of fault breccia and gouge from the Chelungpu Fault Zone [Hashimoto *et al.*, 2007]. (e) Photomicrograph of thin section (in crossed polars) of Rajasthan sandstone (RJS) from India (provided by Takehiro Hirose). (f) Cross-section of micro-CT image of Berea sandstone (BRS) from the U. S. [Dong, 2008].

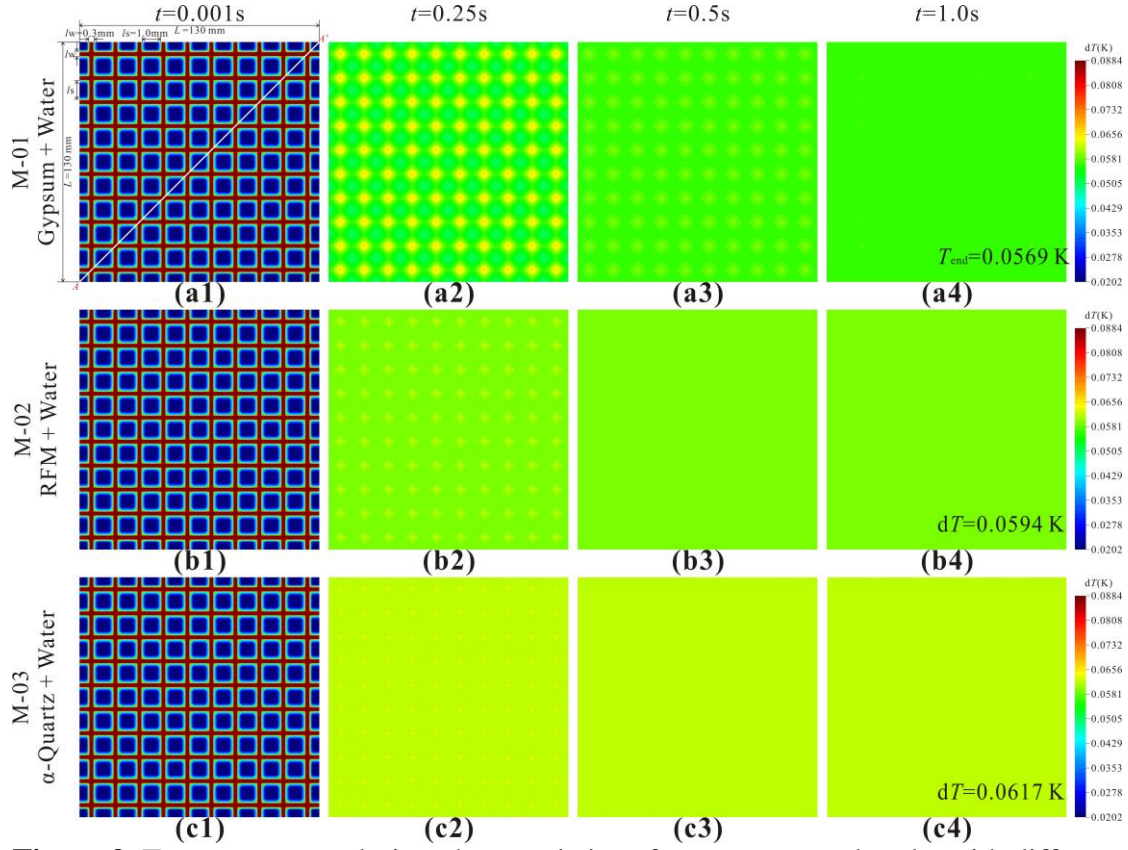


**Figure 9.** Temperature evolution characteristics of water-saturated rocks with different minerals after instantaneous loading from 0 MPa to 10 MPa (i.e.,  $\Delta P_c = 10$  MPa). In models M-01, -02 and -03, the solid grains were gypsum ( $\kappa_{\text{Gypsum}} = 0.51 \text{ mm}^2/\text{s}$ ), main rock-forming minerals averaged (RFM,  $\kappa_{\text{RFM}} = 2.08 \text{ mm}^2/\text{s}$ ) and  $\alpha$ -quartz ( $\kappa_{\alpha\text{-quartz}} = 4.15 \text{ mm}^2/\text{s}$ ), respectively. In these models, each solid grain is surrounded by pore water and the equivalent porosity is up to 0.408 (i.e.,  $\phi = 0.408$ ) since the sizes of grains and pores are set to be 1.0 mm and 0.3 mm, respectively. Each model was meshed to 11025 quadrilateral elements with the spatial resolution of 0.2 mm for grains and 0.06 mm for pores, respectively. The time resolution is up to  $dt = 0.001$  s. (a1-a4) Temperature distribution in model M-01 at  $t = 0.001$  s, 0.25 s, 0.5 s and 1.0 s, respectively. (b1-b4) Temperature distribution in model M-02 at  $t = 0.001$  s, 0.25 s, 0.5 s and 1.0 s, respectively. (c1-c4) Temperature distribution in model M-03 at  $t = 0.001$  s, 0.25 s, 0.5 s and 1.0 s, respectively. The temperature profiles along line A-A' in the three models at  $t = 0.001$  s, 0.25 s, 0.5 s, 0.75 s and 1.0 s, are illustrated in Figure S2.



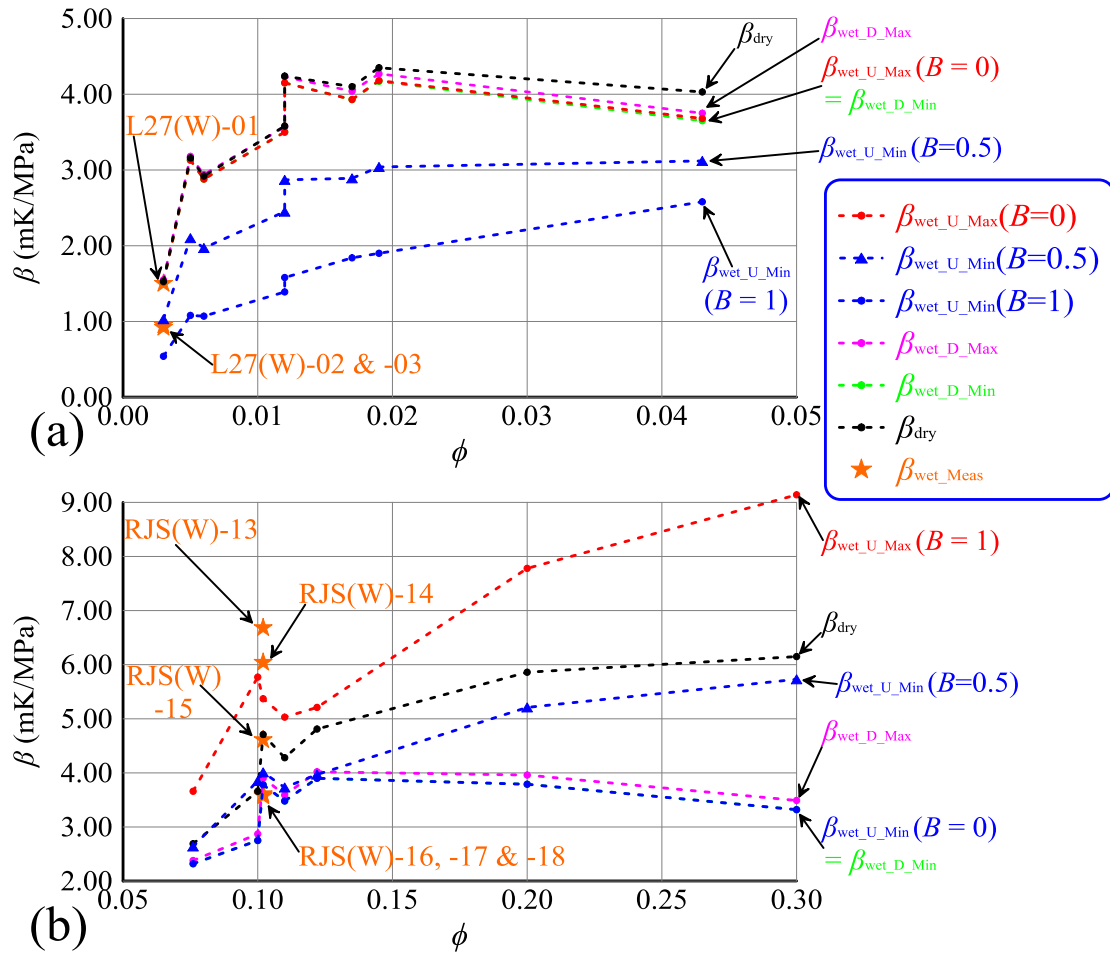


**Figure 10.** Calculated lower and upper limits of  $\beta_{wet}$  for all 15 rock samples when (a) Porosity ( $\phi$ ) is within 0.05 and (b) porosity ( $\phi$ ) ranges from 0.05 to 0.30. Red and pink circles represent the upper limits under undrained ( $\beta_{wet\_U\_Max}$ ) and drained ( $\beta_{wet\_D\_Max}$ ) conditions, respectively. Blue and green circles represent the lower limits in both undrained ( $\beta_{wet\_U\_Min}$ ) and drained ( $\beta_{wet\_D\_Min}$ ) conditions, respectively. Pink dots represent  $\beta_{wet\_U}$  when  $B$  is 0.5 ( $\beta_{wet\_U}(B=0.5)$ ). Blue triangles represent the lower limit under undrained conditions with Skempton's coefficient  $B = 0.5$ . Black circles represent the measured  $\beta$  of dry rocks ( $\beta_{dry}$ ) [Yang *et al.*, 2017]. Orange stars denote measured values of  $\beta_{wet}$  in tests RJS(W)-13 to -18 and L27(W)-01 to -03.